Geochemical evolution and alteration styles of the Gawler Range Volcanics, South Australia

Thesis submitted in accordance with the requirements of the University of
Adelaide for an Honours Degree in Geology

Jesse Hill

November 2019

THE UNIVERSITY
of ADELAIDE

GEOCHEMICAL EVOLUTION AND ALTERATION STYLES WITHIN THE GAWLER RANGE VOLCANICS, SOUTH AUSTRALIA

GEOCHEMISTRY AND ALTERATION WITHIN THE GAWLER RANGE VOLCANICS

ABSTRACT

The Gawler Range Volcanics (GRV) form part of a Mesoproterozoic Silicic Large Igneous Province (Gawler SLIP) within South Australia. The SLIP includes intrusive and extrusive rocks within the Gawler Craton and Curnamona Province that are dominantly felsic. Recent high precision dating of several GRV units has shown that they erupted between 1587 Ma and 1595 Ma allowing for geochemical comparisons with respect to a precise timeline. Trace element geochemistry has shown anomalies to be consistent through the lower and upper GRV demonstrating the main source in the GRV likely did not change. A mafic component is shown to have contributed to both the lower and upper GRV system. Eu anomalies and trace element geochemistry shows that there was a large change in magmatic evolution between the upper and lower GRV within a short time (<1 m.yr). This change is hypothesised to have occurred due to the tectonic regime during the SLIP emplacement. Hydrothermal alteration associated with the emplacement of the Gawler SLIP is known to have contributed to the formation of Iron-Oxide Copper-Gold (IOCG) and shear-hosted deposits in South Australia. More recent discoveries with in the Southern Gawler Ranges display epithermal-porphyry characteristics associated with alteration in the lower GRV. Alteration within the GRV is hereby characterised in order to identify alteration associated with mineralisation. Alteration is shown to encompass a sericite – hematite dominated assemblage which has affected most of the GRV. Several other anomalous alteration assemblages exist in localised areas. Using direct evidence it is suggested that epithermal-porphyry systems may be preserved within the upper GRV, which encompasses a larger outcrop area than the lower GRV which is underexplored.

KEYWORDS

TABLE OF CONTENTS

LIST OF FIGURES AND TABLES

1. INTRODUCTION

Large Igneous Provinces (LIPs) are voluminous deposits of magma that were injected in short (1-5 m.y.) pulses into the crust or erupted at the surface within a relatively short time frame (<50 m.y Bryan et al., 2008). They are located within both intra-plate and plate boundary settings. LIPs are generally mafic and include flood basalts, giant dyke swarms and layered intrusions, while silicic large igneous provinces (SLIPs) are less common, containing over 80% vol. felsic dacitic and rhyolitic units (Bryan et al., 2013). Examples of the latter include the Sierra Madre Occidental of Mexico, the Chon-Aike Province of Southern South America (Pankhurst et al., 1998), the Whitsunday Volcanic Province of Eastern Australia (Bryan, 2007) and the Mesoproterozoic Gawler SLIP of southern Australia (McPhie et al., 2008).

The Mesoproterozoic Gawler SLIP (Figure 1) forms part of the Southern Australian Craton (Allen et al., 2008). It is preserved in the Gawler Craton in central South Australia and in the Curnamona Province in western South Australia, separated by the Neoproterozoic Adelaide Rift Complex (Daly, 1998; Fanning et al., 1988). The Gawler SLIP is composed of the Gawler Range Volcanics (GRV) in the south-central Gawler Craton, and the Benagerie Volcanic Suite (BVS) in the Curnamona Province. These voluminous extrusives were associated with synchronous granitic and minor mafic emplacement of the Hiltaba Suite (HS) granitoids (1595 – 1575Ma) in the Gawler Craton and the Ninnerie Supersuite (1600 – 1570Ma) plutonic rocks in the Curnamona Province (Allen et al., 2008; Allen et al., 2003; Curtis et al., 2018; Wade et al., 2012). The GRV is divided into the lower GRV and upper GRV based on geographical distribution and compositional and textural differences of the units within the GRV (Blissett, 1975, 1986; Fanning et al., 1988; Giles, 1988).

Previous U–Pb zircon dating of upper and lower GRV units yielded ages of 1591 ± 3 and 1592 ± 3 respectively (Creaser, 1995; Fanning et al., 1988), which are not useful in determining meaningful timing relationships of lower and upper GRV eruptions.
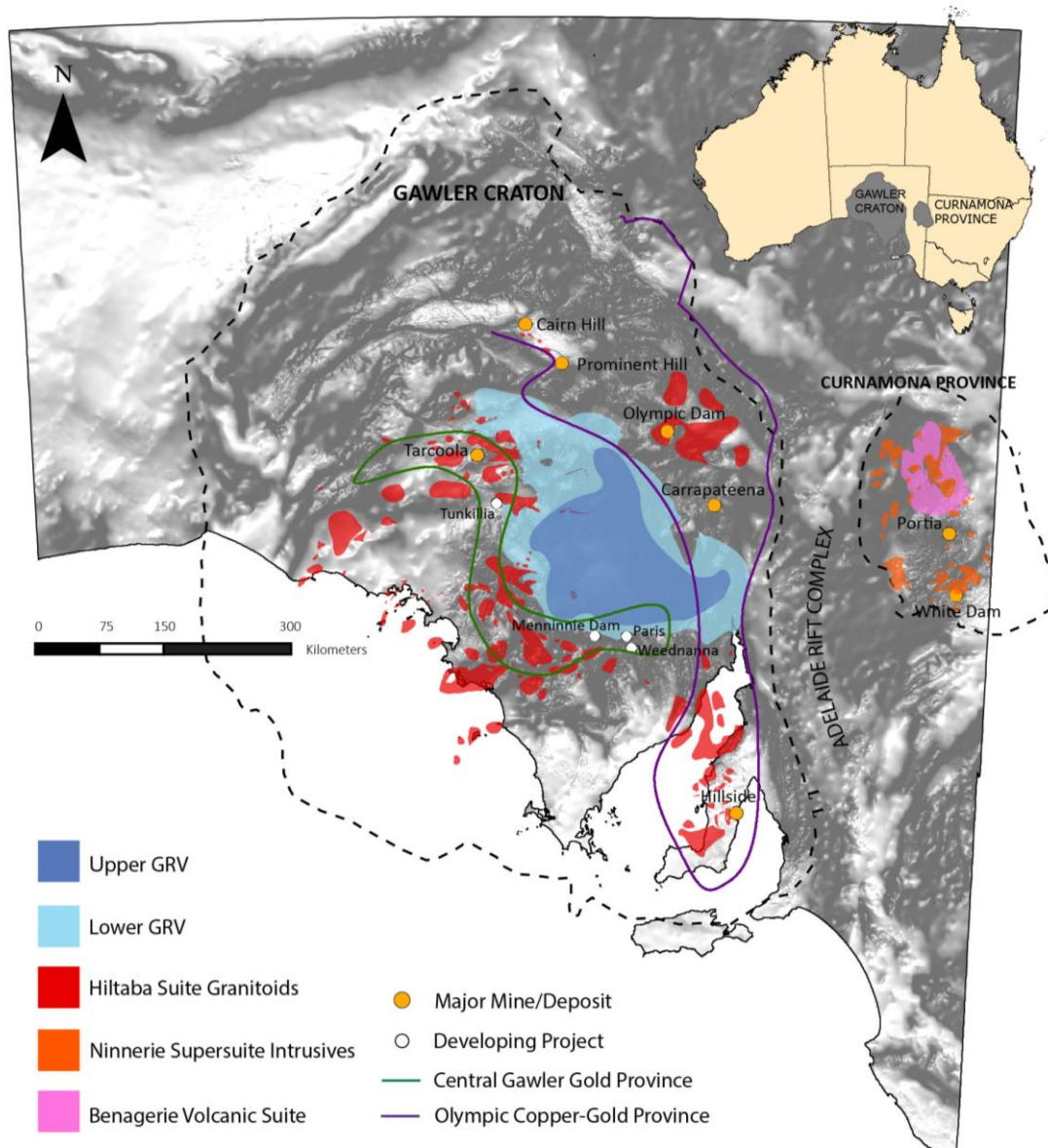
Figure 1: Regional map of South Australia showing the Gawler Range Volcanics (Blue), Hiltaba Suite Granites (Red), Ninnerie Supersuite intrusives (Orange) and Benagerie Volcanic Suite (Pink). Also shown are the boundaries of the two cratons (Gawler and Curnamona Province) and the positions of some of the major deposits and prospects mentioned in this thesis.

Recent high precision dating of the GRV shows that they were erupted between 1595 and 1587 Ma and provides much greater precision for the timing of eruption of several major units within the GRV (Jagodzinski et al., 2016).

The Gawler SLIP is known to be associated with metallic deposits at all scales. The most well-known mineralised area is the Olympic Copper Gold Province (OCGP) which hosts the Olympic Dam, Prominent Hill, Carrapateena and Hillside deposits (Figure 1; Fairclough, 2005; Heithersay 2002). These deposits are considered to be temporally and spatially linked to a large-scale pervasive magmatic hydrothermal event associated with the emplacement of the Gawler SLIP (Skirrow et al., 2007). The Central Gawler Gold Province (CGGP) that hosts the Tarcoola and Tunkillia deposits (Figure 1) is currently a less economically significant region that displays a different style of mineralisation from the IOCG deposits in the OCGP (Fraser et al., 2007). The CGGP is also associated with the Gawler SLIP emplacement, displaying the variation of deposit types created by this event across the southern Australian Craton (Nicolson et al., 2017). More recent deposit discoveries on the southern GRV margin have uncovered a previously overlooked style of mineralisation that may be directly related to shallow hydrothermal circulation driven by the emplacement of the GRV (Anderson, 2014; Jagodzinski, 2012). Epithermal-porphyry and subvolcanic alteration and mineralisation systems have been identified in this region and open up an opportunity for a new exploration model that may be applied to areas within the GRV (Fabris et al., 2017; Paul et al., 2015). While epithermal-porphyry systems have so far only been discovered at the margin of the lower GRV it is not known whether these systems relate to upper or lower GRV emplacement (Fraser et al., 2007; Nicolson et al., 2017).
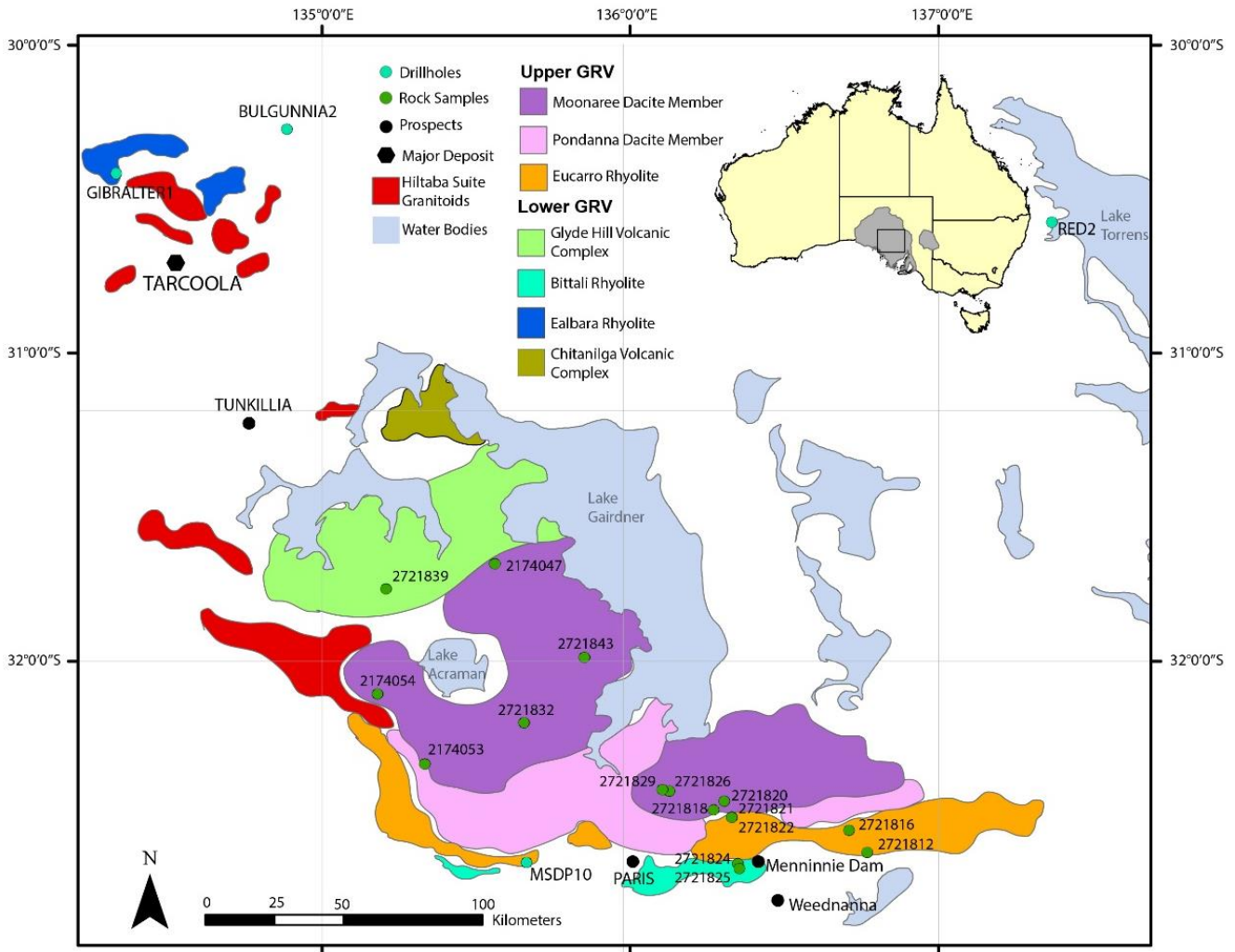
Figure 2: Simplified map of outcropping Gawler Range Volcanics showing locations of field samples and drillhole locations as well as several significant deposits and prospects.

This research aims to use new high precision dates (Table 1) as a timeline to further understand the magmatic evolution across regionally extensive lava units in the GRV. It will investigate six units that encompass a large time span across the eruption of the GRV, however, it is noted that there do exist several lithologies that have not been recently dated using the high precision method and are not analysed here. It will use geochemical and trace element data as well as previously published Sm-Nd isotope data to assess the geochemical differences and the relative input of mantle and crustal sources between the upper and lower GRV units. Different types of hydrothermal alteration across the upper and lower GRV will also be analysed in order to characterise the range of alteration and mineralisation systems

found associated with the GRV, with possible implications for exploration in the central

Gawler Craton.

GRV Unit	Upper/lower GRV	Age (Ma)	Error (2σ)
Red 2 Dacite	Lower	1593.6	0.4
Ealbara Rhyolite	Lower	1591.2	0.5
Bittali Rhyolite	Lower	1589.3	0.5
Mangaroongah Dacite	Lower	1587.7	0.6
Eucarro Rhyolite	Upper	1587.5	0.6
Moonaree Dacite Member	Upper	1587.2	0.5

Table 1: Ages of GRV units studied in this thesis (from Jagodzinski 2016).

2. GEOLOGICAL SETTING

The Gawler SLIP overlies a basement of Archean to Paleoproterozoic units that have been

deformed and metamorphosed up to granulite facies (Hand et al., 2007; Hand et al., 2008).

The oldest exposed basement unit in the Gawler Craton is the Mesoarchean Cooyerdoo

Granite (3150 Ma). It is exposed in the northern Eyre Peninsula and likely extends beneath

much of the central Gawler Craton (Curtis et al., 2019; Fraser et al., 2010). Neoarchean-

earliest Paleoproterozoic (2550-2500 Ma) volcanosedimentary rocks overlie the Mesoarchean

basement in two belts known as the Mulgathing Complex and Sleaford Complex (Hand et al.,

2007). These complexes likely represent a formerly contiguous basin system that is now

separated at surface by younger sediments and the GRV. (Daly, 1998; Hand et al., 2007; Reid

et al., 2012; Swain et al., 2005). A 500 m.y. period of geological quiescence was followed by

a period of basin formation from ca. 2000 to 1730 Ma across the entire Gawler Craton

(Fanning et al., 2007; Reid et al., 2017). Basin formation was punctuated by magmatism of

the Donington Suite at ca. 1850 Ma and ended with the ca. 1730-1690 Ma Kimban Orogeny

when magmatism took over as the main rock-forming process (Hand et al., 2007; Reid et al.,

2008). Post 1690 Ma only minor sedimentary packages were preserved (Fanning et al., 2007).

Following this was a long (ca. 1635-1575 Ma) magmatic episode that began with the ca. 1630

Ma Nuyts Volcanics and ca. 1635-1608 Ma St Peter Suite (Hand et al., 2007; Reid et al.,

2017; G Swain et al., 2005). Following this was a widespread SLIP event encompassing the

Hiltaba Suite granitoids, Gawler Range Volcanics, Ninnerie Supersuite intrusives and the

Benagerie Ridge Volcanics (Allen et al., 2008; Fanning et al., 2007). This felsic emplacement

was synchronous with localised high temperature, low pressure metamorphism associated

with the Kararan and Olarian Orogenies (Cutts et al., 2011; Hand et al., 2007). The Gawler

Craton was then overlain by various Neoproterozoic sediments (Hou et al., 2011).

While the Gawler SLIP is relatively undeformed, it was emplaced synchronous to local

deformation events which are represented in the Gawler Craton as the Kararan Orogeny

(1600 – 1575 Ma; Cutts et al., 2011) and the Curnamona Province as the Olarian Orogeny

(1610 – 1580 Ma; Forbes et al., 2007). This has led to questions about the tectonic regime of

the South Australian Craton while the Gawler SLIP was emplaced (Hand et al., 2007; Hand

et al., 2008).

3. GAWLER RANGE VOLCANICS

The GRV crop out within the southern Australian Craton across an area of $\approx$25,000km^2

(Allen et al., 2003). They extend to the northeast beneath the late Proterozoic and

Phanerozoic sediments of the Stuart Shelf, expanding the coverage of the GRV to

$\approx$90,000km^2 (Allen et al., 2008; Blissett et al., 1993; McPhie et al., 2008; Wade et al., 2012).

The total volume of the GRV and HS may exceed 70,000km^3 and 30,000km^3 respectively

(McPhie et al., 2008). The GRV is comprised of several (90% vol.) large felsic lava flows

and smaller bimodal sequences (Allen et al., 2008). This volume estimate represents a minimum volume as the GRV have been partially eroded. When combined with the Benagerie Volcanics of the Curnamona Province the original volume would have been much larger (Wade et al., 2012).

Initially described as being welded ignimbrites (Blissett, 1975; Fanning et al., 1988), the GRV are now interpreted as vast lava flows that were erupted effusively from volcanic centres and elongate fissure vents, based on field observations and petrological and geochemical investigations (Agangi et al., 2012; Allen et al., 2008). Amygdaloidal top sections, evenly porphyritic and columnar jointed middle sections and flow banding are some observations that led to an effusive origin (Allen et al., 2008; Garner et al., 1999). There is also a general absence of explosive eruption textures such as tuffaceous layers and broken phenocrysts. Both the upper and lower GRV contain lavas with abundant, euhedral to sub-hedral phenocrysts dominated by feldspars and lesser quartz and mafic minerals (Allen et al., 2008). The groundmass ranges from cryptocrystalline or glassy to holocrystalline. It is hypothesised that the Gawler SLIP was emplaced in an intracontinental back-arc or continental hotspot environment (Agangi et al., 2012; Allen et al., 2003).

The GRV have been divided into an upper and lower sequence based on geochemical, stratigraphic and spatial variation (Allen et al., 2003; Blissett, 1975). The lower GRV crops out in the western and southern margin of the GRV and is composed of bimodal lavas and lesser volcaniclastic deposits erupted from several volcanic centres. It ranges from basaltic to rhyolitic compositions with basalt - andesite ($\approx$10%) subordinate to dacite-rhyolite ($\approx$90%)(Allen et al., 2008). Volcanic centres of the Glyde Hill Volcanic Complex at Lake Everard and the Chitanilga Volcanic Complex at Kokatha (Figure 2) are the best exposed areas of the lower GRV, showing extrusive evidence of magma evolution (basalt $\rightarrow$ andesite $\rightarrow$ dacite $\rightarrow$ rhyolite)(Allen et al., 2008). The upper GRV is composed of several

voluminous, felsic lava flows that crop out over a greater area than the lower GRV (Figures 1 & 2). The upper GRV is composed of the Eucarro Rhyolite and Yardea Dacite. The Yardea Dacite is divided into the upper Moonaree Dacite Member and the lower Pondanna Dacite Member while the Eucarro Rhyolite itself includes units of varying textures and compositions (Allen et al., 2002).

The GRV overall has varied major and trace element and Sm–Nd isotope geochemistry. The basalts of the lower GRV have $\varepsilon_{Nd(1580Ma)}$ values between -7.0 and 2.5 (Fricke, 2005; Giles, 1980; Stewart, 1994 unpublished) and are enriched in high field strength elements (HSFE) (Huang et al., 2016). Rhyolites of the lower GRV are enriched in HFSE, Y, rare earth elements (REE), Rb and F (Agangi et al., 2012) and have $\varepsilon_{Nd(1580Ma)}$ values of -7.0 to 1.2 (Stewart, 1994). The upper GRV is silica rich (>65 % SiO_2) and enriched in HFSE and REE. It has $\varepsilon_{Nd(1580Ma)}$ values between -5.4 and 1.8 (Stewart, 1994 unpublished), suggesting a largely crustal origin (Stewart, 1994 unpublished; Wade et al., 2012).

Alteration is common across the Gawler Craton and the GRV is no exception, with variable alteration across most of its units. The ground-mass of most of the GRV units has been variably altered to a pink or red colour by hematite. Feldspars are partially to fully altered by sericite and/or hematite and ferromagnesian minerals are variably altered to chlorite (Giles, 1988). Recent discoveries of epithermal style alteration and mineralisation in the southern margin of the GRV indicate the potential for new exploration models in the GRV unlike the well-known deposit types of the OCGP and CGGP provinces. This alteration includes argillic alteration, silicification, hematite and tourmaline alteration (Wade, 2014) and represents a previously unknown mineralising system associated with the Gawler SLIP. The Paris Ag-Pb prospect is the largest deposit of this style to have been discovered (Paul et al., 2015). It is hosted mainly within the lower GRV and partly within the underlying basement. It shows epithermal vein textures such as colloform banding, comb quartz, bladed quartz after calcite

as well as typical epithermal mineralogies (Paul et al., 2015; Wade, 2014). Recent dating of the alteration associated with mineralisation of Paris and other similar deposits in the region have confirmed that it is in fact a preserved Mesoproterozoic epithermal system (Nicolson et al., 2017; Paul et al., 2015). This leads to the possibility of discovering remnants of a regionally extensive and varied epithermal system/s within the GRV (Nicolson et al., 2017).

4. METHODS

Samples were collected from the field and drill core stored at the South Australian Drill Core Reference Library. Sixteen field samples were chosen for this geochemical analysis that encompass several lower and upper GRV units across the extent of the GRV outcrop area. Several of these samples were taken from the sites that were recently dated by Jagodzinski (2016). The least altered rocks were chosen for the purpose of whole rock geochemistry with the weathered exteriors removed in the field. Two samples were chosen for alteration analysis as they showed possible epithermal alteration. Twenty-five lower GRV samples were collected from four drillholes; Bulgunnia 2, Gibralter 1, Red 2 and MSDP10. Again the least altered samples were chosen for the geochemical analysis while altered samples were chosen for the alteration analysis. These drillhole samples increase the geographical extent of the sampling area to include the GRV beneath the Stuart Shelf. Overall 28 lower GRV and 13 upper GRV samples were collected for both geochemistry and petrographical analysis. Rock samples were processed at the University of Adelaide. Samples were first cut into pieces with any additional weathered pieces removed. The cuttings were then crushed, split and then milled into a fine powder. Sample powders were analysed by Bureau Veritas Minerals, (https://www.bureauveritas.com.au/) Perth, Western Australia using X-ray Fluorescence for major element geochemistry, Laser-ablation Inductively Coupled Plasma

Mass Spectrometry (LA-ICP-MS) for trace elements, Fire Assay ICP MS for Au, Pd and Pt, weight analysis for FeO and Specific ion Electrode for fluorine.

Eighteen 30µm thin sections were made by Adelaide Petrographic Laboratories for petrographical analysis. Several samples and thin section off-cut blocks were further analysed at Adelaide Microscopy to identify several minerals that couldn't be confirmed using petrography. These samples were polished at The University of Adelaide and then carbon coated at Adelaide Microscopy. Samples were analysed by Energy-dispersive X-ray spectroscopy (EDS) by the Quanta 450 SEM (Scanning Electron Microscope) at Adelaide Microscopy. Minerals were identified and confirmed by a combination of petrology and EDS spectra.

5. OBSERVATIONS AND RESULTS

5.1. Sample Descriptions and Field Observations

Samples collected from the field and drill-core library were variable in terms of textures, compositions and alteration. Lower GRV samples included rhyolites and dacites that were all porphyritic with a cryptocrystalline groundmass. Phenocrysts are dominated by plagioclase, k-feldspar, quartz and altered mafic minerals. Phenocryst modal percentages, size and abundance is variable between and within individual units. Alteration is dominated by sericite and hematite (red rock) alteration, but there is considerable variation in some areas especially within the samples drillholes. Upper GRV rhyolites and dacites showed similar mineralogies to lower GRV rhyolites and dacites. Some outcrops showed partially filled amygdales and common mafic enclaves. Representative field and drillhole samples are shown in Figure 3. Representative sample descriptions and comments on each unit are presented in Table 2.

Sample	Unit	Description	Comments
2721820	Moonaree Dacite Member	Red/brown porphyritic rock with 20 % phenocrysts dominated by euhedral plagioclase (<20mm) and k-feldspar (<5mm) with lesser, sub-rounded smokey quartz phenocrysts (<4mm). Feldspars are unevenly altered by quartz and hematite. Altered mafic mineral up to 100mm. Matrix is fine grain crystalline.	There are common mafic enclaves throughout the outcrop. They are sub-rounded and fine grain crystalline (Figure 3a). Up to 50mm in size. Partially infilled amygdales are found in some areas.
2721812	Eucarro Rhyolite	Porphyritic red/brown rhyolite with around 35% phenocryst volume. Phenocrysts are dominated by euhedral plag, K-feldspar. Around 10% mafic altered minerals and lesser sub-rounded quartz.	Outcrop was columner jointed. Phenocryst percentage, size and mineral abundance varies on a 1-10m scale.
2721821	Eucarro Rhyolite, Silicified Sample	Porphyritic rhyolite breccia with stockwork veining. Pale pink/white highly silicified rhyolite with small round quartz phenocrysts and lesser altered feldspar. There is quartz veining with cryptocrystalline silica (chalcedony). Vuggy texture with comb quartz infill.	Breccia and silified alteration textures (vugs, veins, comb quartz) resembles high level epithermal alteration.
2721838	Mangaroongah Dacite	Porphyritic dacite with glassy very fine-grain groundmass and 15-20% phenocrysts of sub-hedral k-feldspar and plagioclase. Dark red/purple iron stained rock with flow banding. Quartz phenocrysts are common and up to 5mm in size.	There are some parts of the outcrop that are less consolidated containing clasts of differing compositions and amounts of flowbanding. Possible indication of a pyroclastic origin.
2721825	Bittali Rhyolite	Pink/red rock with 40% phenocrysts. Rounded 2-4mm quartz crystals are dominant followed by euhedral k-feldspar and plagioclase. Groundmass is fine grain quartz/feldspar. Some minerals are completely altered and weathered to sericite and clays.	Typical alteration seen throughout the Gawler Ranges. Similar to Figure 3c without pyrite.
2746124	Bittali Rhyolite MSDP 10 Drillhole	Pale green/grey rhyolite with 20-50% phenocrysts. Subrounded quartz to 3mm is dominant followed by altered feldspars. Feldspars and groundmass is altered to pale green by chlorite, sericite and epidote? Some sulphide mineralisation present. Fluorite is found within some quartz veins.	Alteration contains sulphides and is atypical of GRV alteration seen elsewhere.
2729182	Ealbara Rhyolite Bulgunnia 2 Drillhole	Red/brown porphyritic rhyolite with 10-30% phenocrysts. Phenocrysts are dominated by sub-rounded quartz followed by k-feldspar and plagioclase. Dark altered (previously mafic?) minerals are common up to 3mm in size. Stockworks of small fractures and veins with silicic and sericitic alteration extending from fractures.	Background alteration appears to be typical red rock alteration, however, silicic stockwork veining and alteration appears to represent another stage of hydrothermal alteration (Figure 3d).
2729180	Ealbara Rhyolite Gibralter 1 Drillhole	Red/brown porphyritic rhyolite with variable phenocryst size and abundance. Phenocrysts are 50% sub-rounded quartz and 50% variably altered, sub-hedral felspars. The groundmass is flow banded with convolute bands of quartz bending around phenocrysts (Figure 3F). Stockworks of small quartz-calcite veins and fractures with silicic alteration extending from veins. Pyrite is found within the veins and in the groundmass in some areas.	Flow banding may of controlled the movement of fluid through the rock (Figure 3f). Pyrite is associated with the silicic veining and alteration which is similar in appearance to the Bulgunnia 2 drillhole.
2729187	Red 2 Dacite Red 2 Drillhole	Red/brown – green porphyritic dacite with 20-50% phenocrysts. Phenocrysts are dominated by euhedral plagioclase followed by k-feldspar up to 5mm in size. Mafic minerals have been chloritized. Alteration include typical hematite alteration and zones of overprinting chlorite dominated alteration. Late stage veins contain quartz-hematite with hematite alteration extending from the veins. Sulphides are found within the groundmass associated with chloritized mafic mineral aggregates and	There seems to be at least 3 episodes of alteration with the first being the typical red rock alteration followed by a chlorite dominated alteration, followed by late stage quartz-hematite dominated veining and alteration.

Table 2: Field observations and sample descriptions that are representative of the units analysed in this study. There are more than one entry for units where samples varied significantly either texturally, compositionally or in terms of alteration.
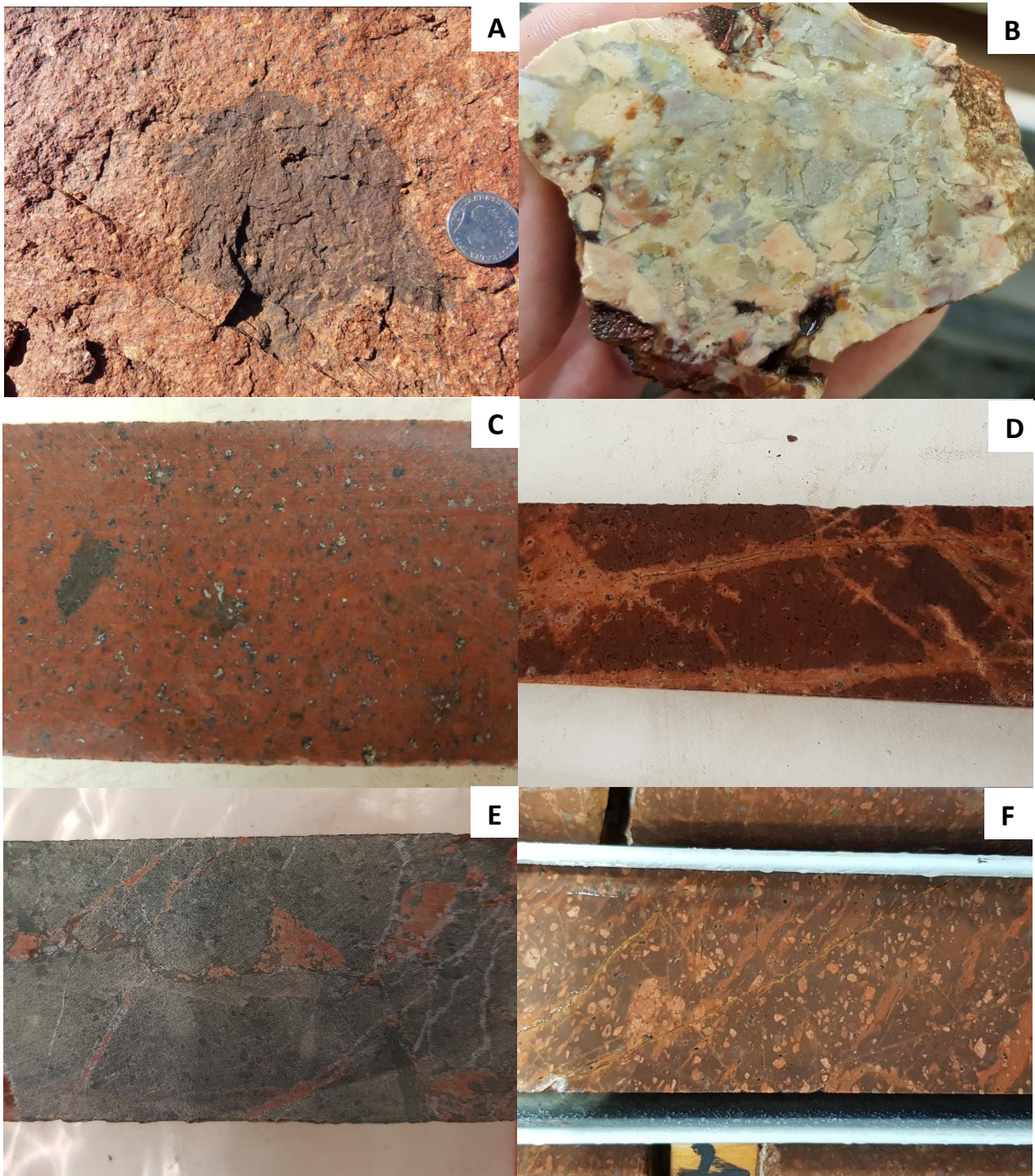
Figure 3: a) Mafic enclave found within in the Moonaree Dacite Member. **b)** Highly silicified breccia with a vuggy texture found within the Eucarro Rhyolite. **c)** Hematite altered sample of Red 2 Dacite from the Red 2 drillhole showing pyrite mineralisation. **d)** Ealbara Rhyolite sample from the Bulgunnia 2 drillhole showing hematite alteration and overprinting silicic veining and alteration. **e)** Drillcore sample of the Red 2 Dacite showing brecciation, veining and multiple types of alteration (chloritic and hematite). **f)** Flow banding in a red-rock altered drillcore sample of Ealbara Rhyolite in the Gibralter 1 drillhole.

5.2. Geochemical Results

5.2.1. MAJOR ELEMENTS

38 samples were collected and analysed for whole rock and trace element geochemistry with

9 of those samples representing highly altered lithologies intended for use in the alteration

analysis of this study.

The 29 unaltered samples plot in the rhyolite and dacite fields on the Total Alkalis Silica

classification diagram (Fig 4). Figure 4 shows that both the upper and lower GRV contain

dacitic and rhyolitic units.
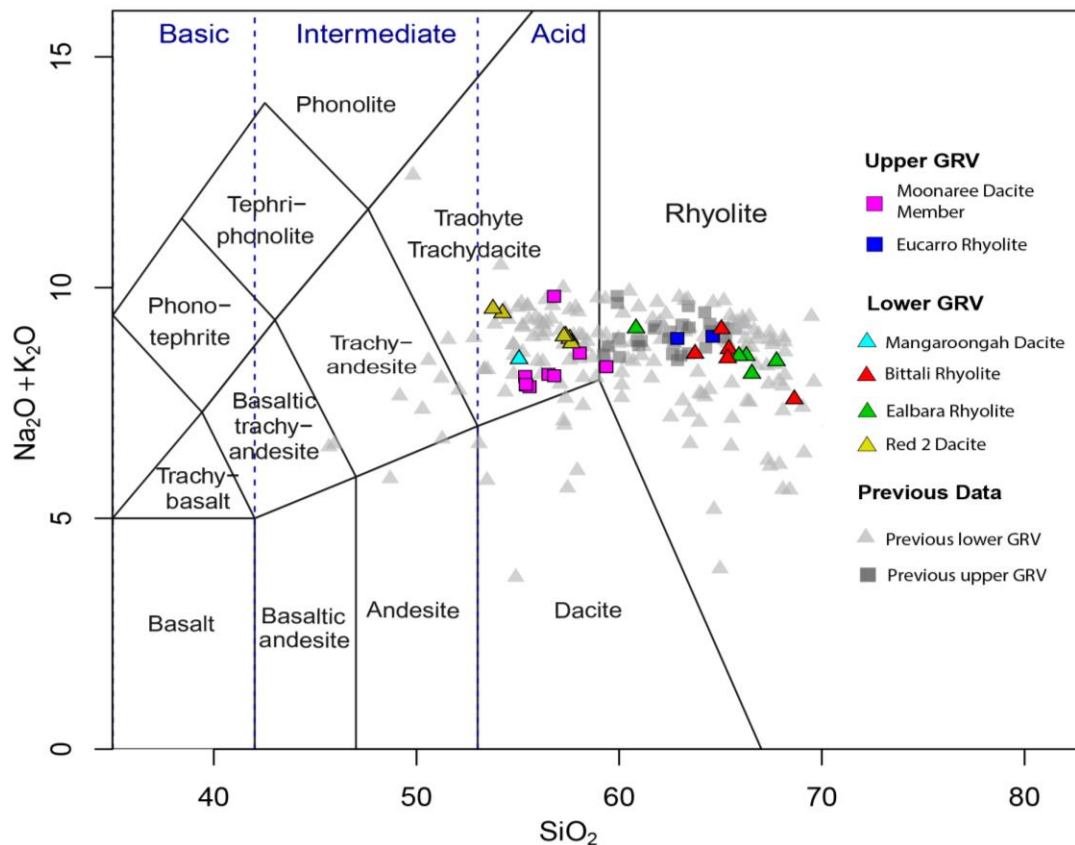
Figure 4: Classification of GRV samples with total alkalis (Na$_2$O + K$_2$O) are plotted against silica (SiO$_2$) – TAS Diagram (Le Bas et al 1986). Shapes correspond to upper GRV (squares) and lower GRV (triangles).

Major elements oxides plotted against SiO$_2$ show negative trends for Al$_2$O$_3$, CaO, MgO,

P$_2$O$_5$, TiO$_2$ and FeO$_{(total)}$ (Fig 5). Na$_2$O and K$_2$O show no obvious trend. In general, the upper

GRV has less variation in SiO$_2$ ranging from 64 to 73 wt%, while the lower GRV has a larger

spread in SiO_2 from 64 to 78 wt% SiO_2 (Figure 5). The upper GRV also shows less variation in Al_2O_3, P_2O_5 and TiO_2. The range of values in MgO, Na_2O and $FeO_{(total)}$ is consistent between both upper and lower dacites and rhyolites. Dacites of both the upper and lower GRV display similar major oxide compositions with the only notable differences being a higher CaO content in the upper GRV Moonaree Dacite Member than the lower GRV Mangaroongah Dacite followed by the Red 2 Dacite (lower GRV). The Red 2 Dacite has a generally higher K_2O content and lower Na_2O content than the Mangaroongah Dacite and Moonaree Dacite Member. The rhyolites of the lower GRV display similar major oxide compositions to those in the upper GRV with the only distinguishing feature being that the lower GRV rhyolites have higher SiO_2 values (average 74.6wt%) than the upper GRV (average 72.6wt%).

5.2.2.   TRACE ELEMENTS

The trace element geochemistry of the samples is presented in Appendix A and Figures 6-8. Inflections are seen at approximately 67-68wt% SiO_2 in Ba, La, and Sr; although some are quite broad due to variation in samples. Broad inflections at 71-72% SiO_2 are shown in the Y and Zr plots. Some distinct groups are formed within the dacites in some plots while the rhyolites are generally more randomly distributed. The Red 2 Dacite (lower GRV) has consistently higher Th than the Moonaree Dacite Member (upper GRV) followed by the Mangaroongah Dacite (lower GRV) with the lowest Th value across a similar SiO_2 range. This trend is repeated in La and Rb, and the opposite trend is observed in the Sr plot. The plotted rhyolites show a much higher degree of variation amongst some trace elements (Figure 6). On the primitive mantle normalised trace element diagram (Figure 8) large ion lithophile elements (LILE) are comparatively enriched to the high field strength elements (HFSE) with negative anomalies in Ba, Nb, Sr, P, Eu, Ti and a positive anomaly at Pb (Figure

8). These anomalies are highly variable between units and samples within units, particularly

in Ba, Sr and P. On the chondrite normalised REE diagram there is a general decreasing

trend, with a steep negative slope in the light REE and an almost flat slope in the heavy REE
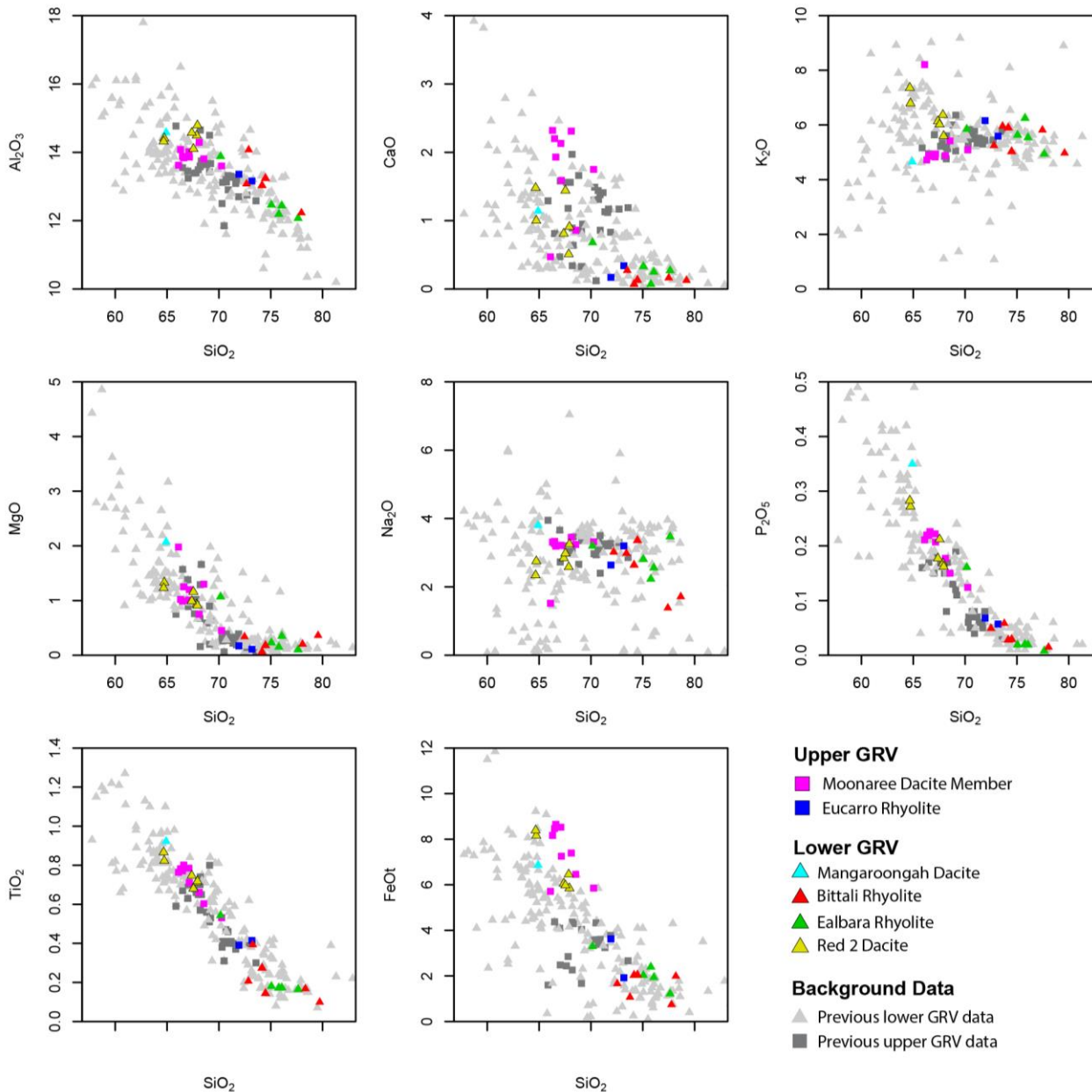
Figure 5: Major element oxides versus SiO₂ (Harker Diagrams). New data is coloured according to individual units. Background data is previous data collected from the GRV; upper GRV = grey squares, lower GRV = grey triangles. Previous data from Agangi, 2011; Giles, 1980; Jagodzinski, 1985; Stewart, 1994 unpublished; and South Australian Resources Information Gateway (SARIG)

(Figure 9). The rhyolites show a wider range in element values with no obvious

distinction between upper and lower rhyolites. The dacites show less variation and in general

are similarly enriched in all REE other than Eu. Dacite and rhyolite Eu anomalies (Eu/Eu*)

range from 0.15 to 0. 85 with an average of 0.62. The three rhyolites have larger negative Eu

anomalies (0.40) than the dacites (0.71).
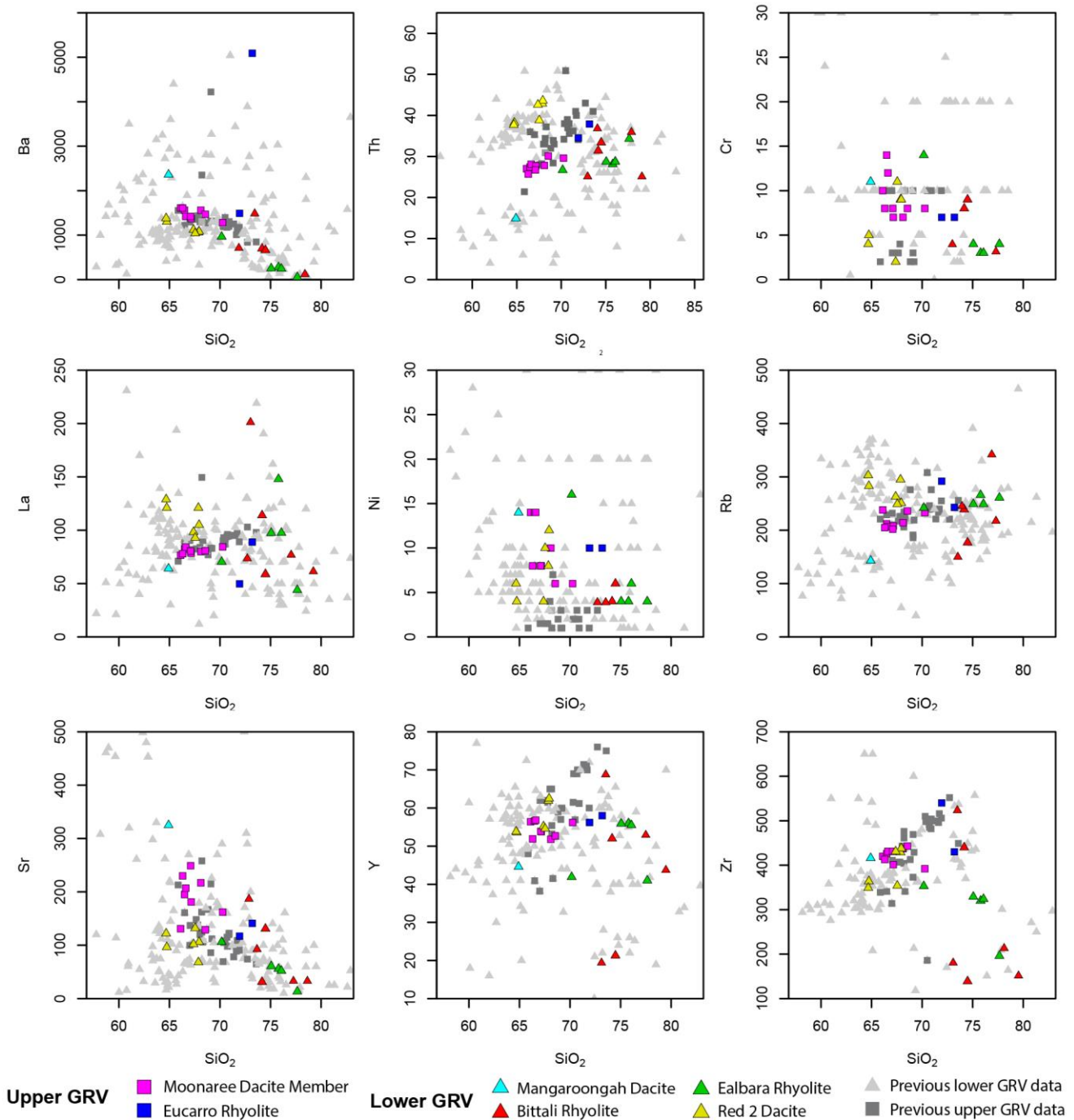
Figure 6: Trace element versus silica (SiO₂) diagrams. Inflections are seen at 63-64% SiO2 in Ba, Ce, La & Sr; at 71-72% in Y & Zr. Ni and Cr have seemingly random distributions overall, however, groups are formed in the data that are repeated in multiple plots. Previous data from Agangi, 2011; Giles, 1980; Jagodzinski, 1985; Stewart, 1994; and South Australian Resources Information Gateway (SARIG)

$(La/Sm)_N$ values range from 2.5 to 6 for the whole data set and averages are around 4 to 5 with the exception of the Mangaroongah Dacite which has an average of around 3.2 (Figure 7). All units have large spreads in $(La/Sm)_N$ with the exception of the Moonaree Dacite Member which has a spread of less than 1. $(La/Sm)_N$ is seen to decrease throughout the eruption of the lower GRV followed by a comparatively sudden increase at the onset of the upper GRV. Eu/Eu* anomalies are all negative and range from 0.1 to 0.9 for the lower GRV and 0.48 to 0.7 in the upper GRV highlighting the significant spread of Eu anomalies within the lower GRV (Figure 7). In general, the dacites have a much lower spread in Eu/Eu* values than the rhyolites.
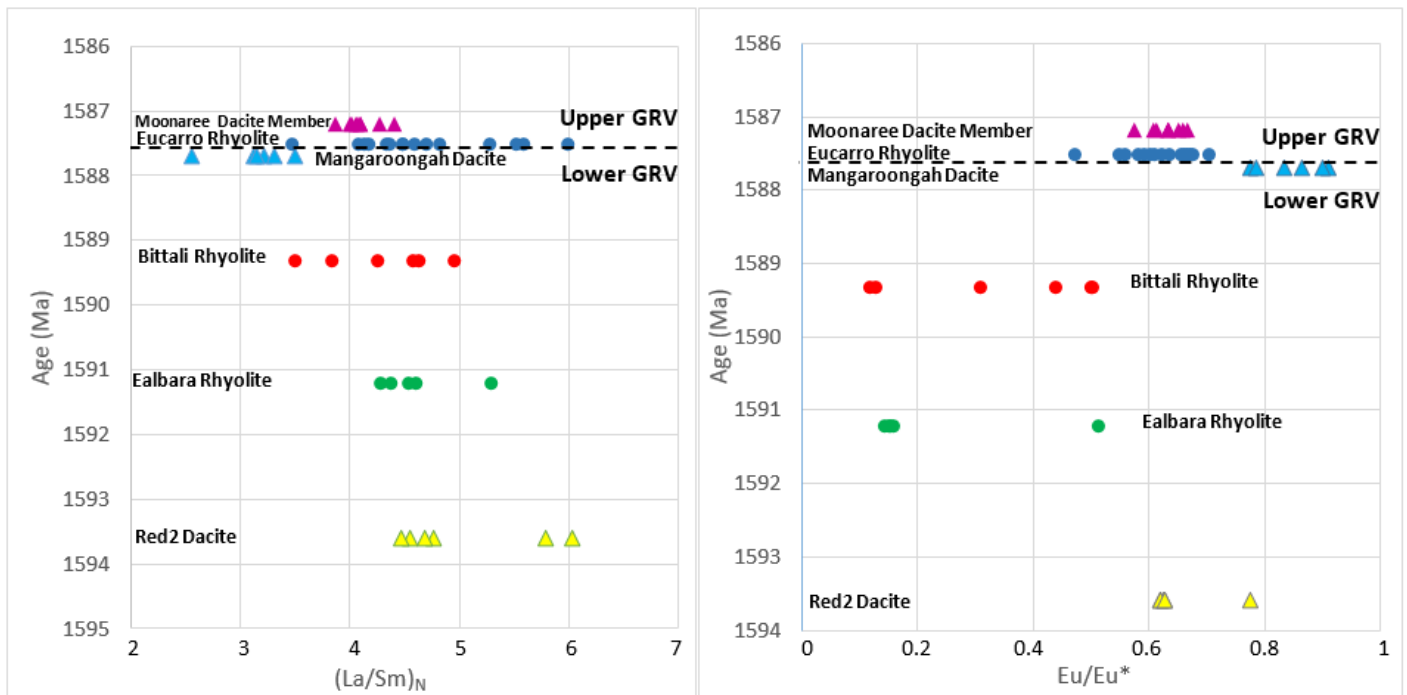
Figure 7: Graphs of age versus $(La/Sm)_N$ values and Eu/Eu* anomalies of the 6 units analysed in this study. The graphs are arranged as a stratigraphic column. Supplementary existing data was added to the Mangaroongah Dacite and Eucarro Rhyolite as there were only one and two samples respectively from these units analysed in this study (from SARIG). Normalising values are from Sun and McDonough (1989).
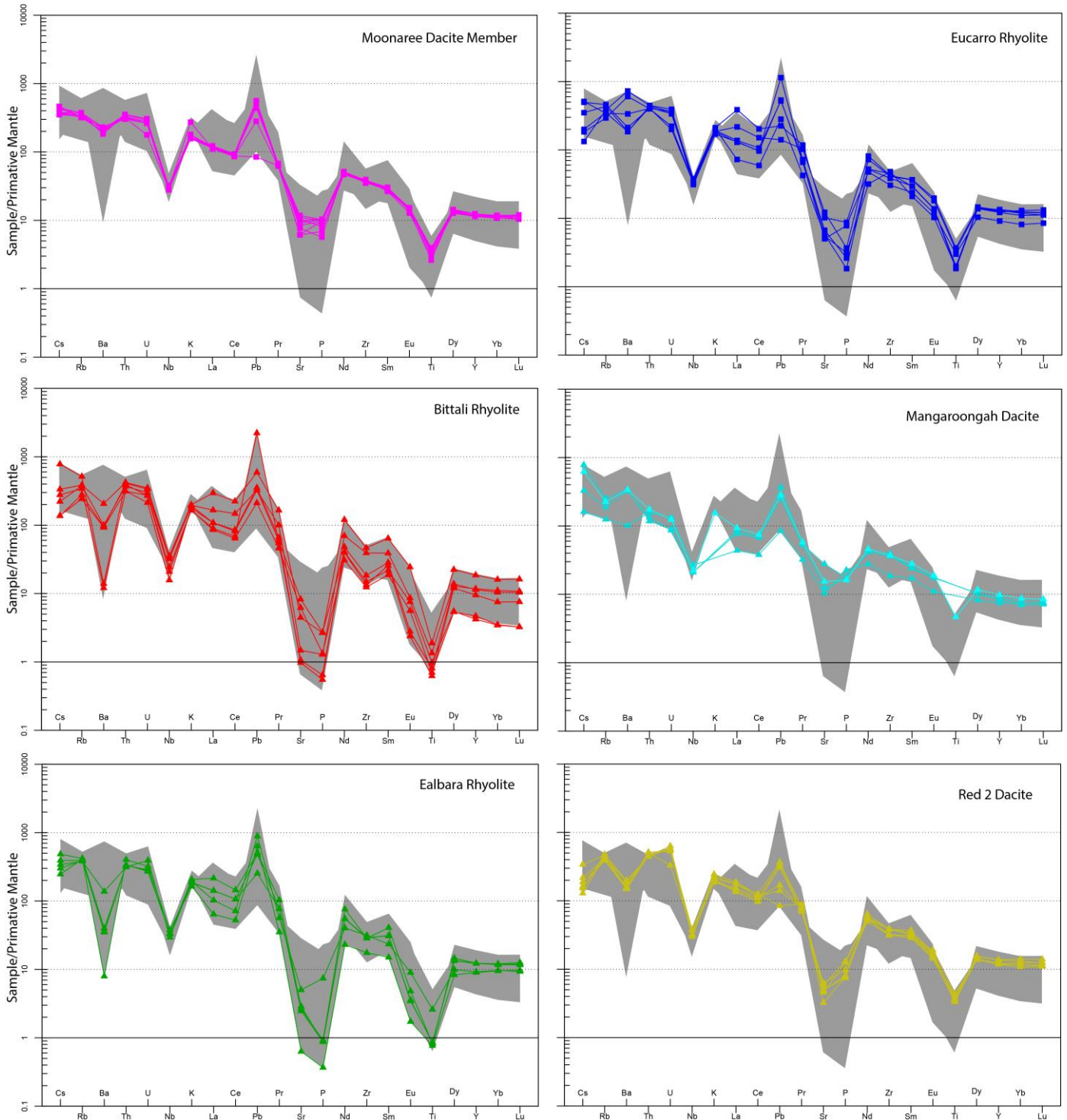
Figure 8: Primative mantle normalised trace element diagram. Upper GRV units are squares. Lower GRV units are triangles. There are significant depletions in Ba, Nb, Sr, P, Eu and Ti. There is a general decreasing trend from Cs to Lu and a positive anomaly at Pb. Grey Field is the whole data set. Supplementary existing data was added to the Mangaroongah Dacite and Eucarro Rhyolite as there were only one and two samples respectively from these units analysed in this study (from SARIG). Primitive mantle normalising values from Sun & McDonough (1989).
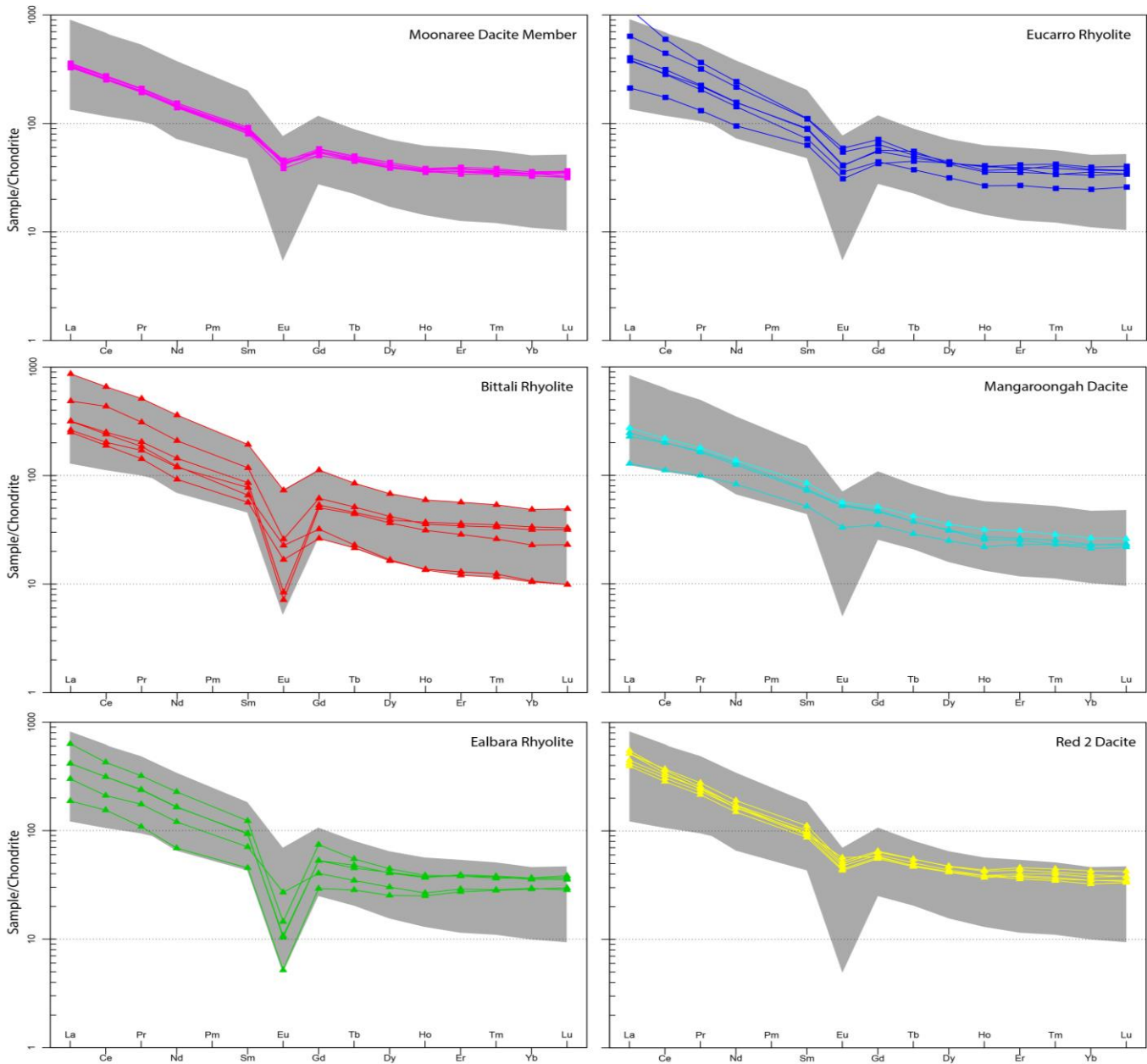
Figure 9: Rare earth element normalised plots for each GRV unit. Upper GRV units are squares. Lower GRV units are triangles. Grey field is the whole data set. Supplementary existing data was added to the Mangaroongah Dacite and Eucarro Rhyolite as there were only one and two samples respectively from these units analysed in this study (from SARIG). Chondrite normalising values from Taylor and McLennan (1985).

5.3. Alteration in the GRV

Nineteen samples of various units, areas and alteration styles were selected for petrographic

analysis. Seven samples were further analysed using a Scanning Electron Microscope (SEM)

for EDS spectra to identify and confirm the different mineral assemblages seen during

petrological analysis. The main petrographic descriptions modal abundances and alteration

assemblages from petrology and EDS are presented in Table 3.

22

Sample	Petrological description	Modal abundances		Alteration assemblage (Petrology + EDS)	Interpreted Alteration Type
2729189 – Red 2 Dacite -Lower GRV	Plagioclase and alkali feldspar (up to 10mm) are the dominant phenocrysts and display anhedral to euhedral grain shapes. Perthitic feldspar textures are common and multiple twinning in plagioclase is observed where alteration is less intense. Feldspars are variably altered to sericite and hematite with sericite being more closely associated with plagioclase while hematite is more prevalent in the alkali feldspar grains. Pyrite is common and is associated with dark aggregates of iron oxide and chlorite. Other common alteration minerals include chlorite, iron oxide (opaque), dolomite and minor fluorite. These minerals represent an assemblage that are spatially associated and form aggregates.	**Phenocrysts: 50%** Alkali Feldspar – 30% Plagioclase – 50% Quartz – 15% Pyrite – 2%	**Groundmass: 50%** Alkali Feldspar – 40% Quartz – 40% Plagioclase – 20%	Sericite, chlorite, Fe oxide, dolomite ± fluorite ± pyrite	Sericitic/Phyillic
2729183 – Bulgunnia 2 – Ealbara Rhyolite -Lower GRV	Porphyritic rhyolite with a cryptocrystalline groundmass of alkali feldspar and albite. Sub-hedral to euhedral alkali felspars are the dominant phenocrysts (<3mm) and commonly display perthitic textures and simple twinning. The other main phenocrysts are pseudomorphs (<2mm) most likely after mafic minerals, containing felspar, quartz, iron-oxide, chlorite, dolomite ± halite. This assemblage has completely psuedomophed the previous mineral leaving little evidence of what it was, although it presents a sub-hedral tabular grain shape. The K-feldspar is moderately altered to sericite and iron-oxide (hematite). The entire groundmass has been altered by hematite which is concentrated in microfractures and small patches throughout the rock.	**Phenocrysts: 25%** Alkali Feldspar – 80% Psuedomorphs containing K-feldspar, Opaque, Chlorite ± Rutile–20%	**Groundmass – 75%** Alkali feldspar – 50% Plagioclase – 50%	Sericite, Fe-Ti Oxides, chlorite ± dolomite	Phyllic/Sericitic
2729178 – Gibralter 1 Ealbara Rhyolite -Lower GRV	Porphyritic, flow banded rhyolite with convolute layers of very fine grain quartz/feldspar matrix. Quartz s up to 4mm and displays rounded embayed textures. Feldspars are up to 6mm, sub-hedral, are albitised and display perthitic twinning. Feldspars are altered by hematite and chlorite. The chlorite is found mainly within the feldspars but also in fractures within the matrix and displays a pale green colour with low pleochroism. Iron oxide and minor fluorite are also found within many of the altered feldspars. The ground mass is heavily altered by hematite creating a brick red colour.	**Phenocrysts: 40%** Quartz – 50% Feldspars – 50%	**Groundmass: 60%** Quartz/feldspar – 100%	Hematite, chlorite, Fe-oxide, clay	Argillic/Sericitic
2746122 – MSDP 10 Bittali Rhyolite -Lower GRV	Porphyritic rhyolite with a cryptocrytsaline groundmass of mainly quartz and k-feldspar. Phenocrysts are euhedral to sub-hedral with the dominant phenocryst being plagioclase followed by k-feldspar and then quartz and rare amphibole of grain size up to 4mm. The plagioclase phenocrysts show variable chloritoid and sericite alteration and are often completely destroyed. K-feldspar is altered mainly by sericite and chloritoid. Feldspars are often altered to albite, orthoclase and chloritoid. Quartz is sub-rounded and generally un-altered. The groundmass is altered by sericite and chloritoid. A common alteration assemblage is chloritoid, pyrite, iron-oxide, fluorite and chloritoid. Flourite is associated with pyrite often found within the pyrite grain.	**Phenocrysts: 20%** Plagioclase – 40% Potassium feldspar 30% Quartz – 20% Hornblende – 5% Opaque – 1%	**Groundmass: 80%** Quartz – 80% K – Feldspar – 20%	Sericite, albite, chlorite, Fe-oxide ± pyrite ± fluorite	Sericitic/Phyillic
2721839 – Mangaroongah Dacite -Lower GRV	Porphyritic dacite with cryptocrystalline groundmass. Low phenocryst percentage with plagioclase being the dominant phenocryst. The feldspars show sub-rounded and embayed to euhedral textures and are up to 4mm. Quartz shows rounded an embayed textures up to 2mm. Feldspars are altered by hematite and lesser chlorite. Previous mafic minerals have been completely altered to chlorite, iron oxide and a clear, high relief, high pleochroic fine grain mineral. The groundmass is heavily altered by hematite, chlorite and iron oxide.	**Phenocrysts: 10%** Plagioclase – 70% K-feldspar – 150% Quartz – 10% Chlorite – 5%	**Groundmass: 90%** Quartz/feldspar – 100%	Hematite, chlorite, Fe-oxide, clear, high relief mineral	Fe-oxide/Chlorite
2721832 – Moonaree Dacite Member -Upper GRV	Cryptocrystalline groundmass comprised of quartz and felspars and are generally anhedral to subhedral. Plagioclase is the dominant phenocryst showing multiple twinning and euhedral grain shapes. K – felspar phenocrysts are often albitised and all feldspars are altered by hematite/sericite alteration. Previously mafic phenocrysts have often been altered to chlorite. The groundmass is pervasively altered by hematite. Chlorite, epidote, titanite and Ti-oxide have also grown as a result of alteration and are commonly spatially associated. Apatite is common as an accessory phase. Yellow mineral, high birefringence mineral	**Phenocrysts: 70%** Plagioclase – 55% K-feldspar – 40% Mafics – 5%	**Groundmass: 30%** K-feldspar – 40% Quartz – 30% Plagioclase – 30%	Sericite, hematite, albite, epidote, titanate, Ti-oxide	Phyllic/Sericitic
2721824 – Bittali Rhyolite -Lower GRV	Porphyritic rhyolite with cryptocrystalline groundmass. The main phenocrysts are plagioclase and k-feldspar which show euhedral grain shapes up to 5mm in size. The quartz phenocrysts are up to 3mm and show rounded embayed textures. The plagioclase phenocrysts show albitisation and irregular multiple twinning. K-feldspar displays perthitic and simple twinning. Feldspars are altered by sericite with patches of dolomite and iron oxide. The groundmass is pervasively altered by needle shaped white micas and iron oxide.	**Phenocrysts – 40%** Plagioclase- 40% K-feldspar – 40%	Quartz – 20% **Groundmass: 60%** Quartz/feldspar 100%	Sericite, Fe-oxide, dolomite	Sericitic
2721821 – Silicified sample – Eucarro Rhyolite - Upper GRV	Silicified porphyritic rhyolite with cryptocrystalline groundmass. Phenocrysts are mostly sub-rounded quartz, up to 2mm in size that displays embayed textures. Previous feldspar phenocrysts up to 1mm are altered completely to quartz and epidote. Fluorite is found throughout in small proportions and inside altered grains. The groundmass is altered by silicic minerals and rutile. There is a quartz vein that shows comb quartz textures and recrystalised silicified alteration extending into the sample from the vein.	**Phenocrysts: 10%** Quartz – 80% Altered feldspars – 20%	**Groundmass – 90%** Quartz – 90% Feldspar – 10%	Quartz, epidote, rutile ± fluorite	Silicic/Outer Propylitic

Table 3: Table of petrological and EDS analysis results for each unit. This is an example of some of the alteration associated with these units. For the full petrological/EDS results see Appendix B & C.

23

5.3.1. PETROGRAPHIC AND EDS RESULTS

Altered samples were analysed using a combination of thin-section petrography and EDS analysis on the SEM. Alteration assemblages were then compared to the hydrothermal alteration table below (Figure 10).
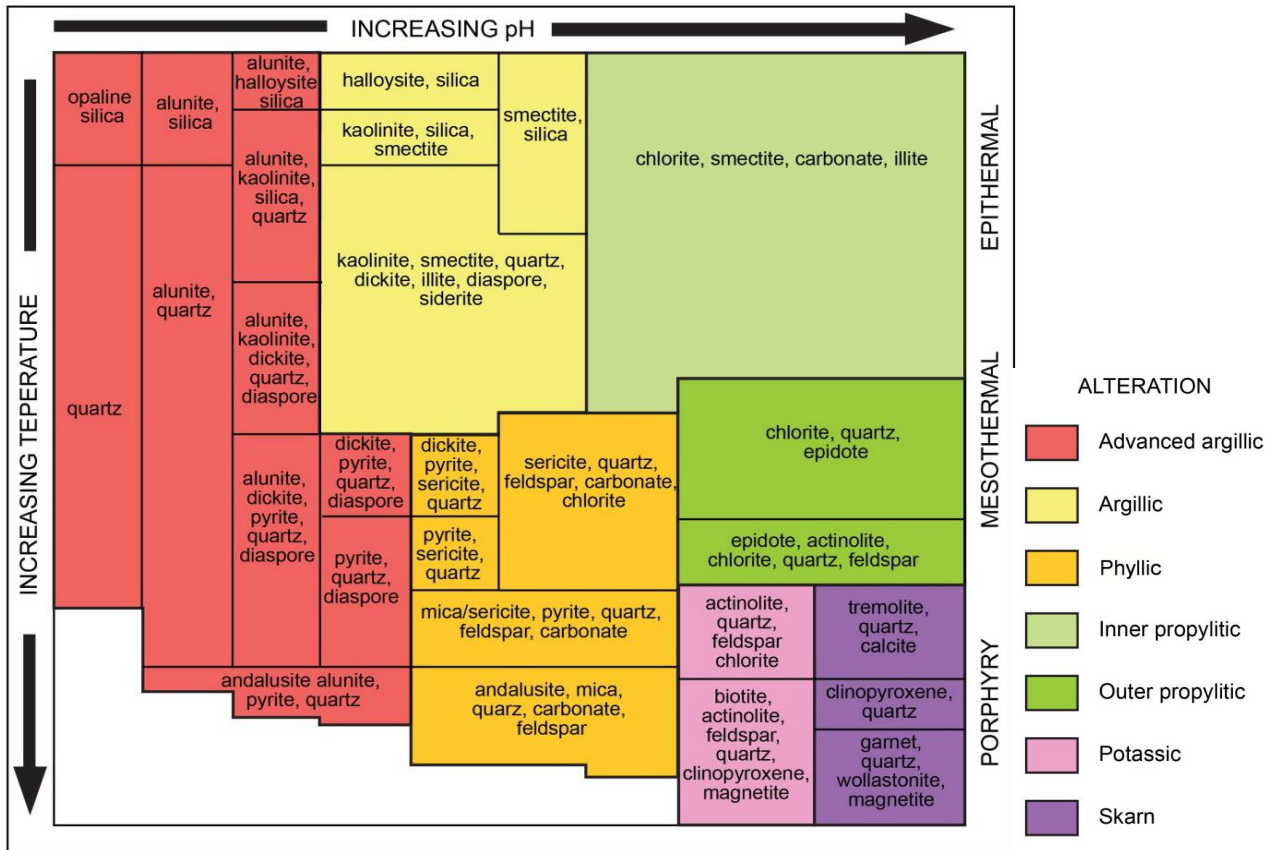
Figure 10: Alteration mineralogy in hydrothermal systems, modified from Corbett and Leach (1998)

5.3.1.1. Red 2 Dacite

The Red 2 Dacite is the oldest dated GRV and is concealed beneath 300m of Stuart Shelf sediments. It showed differing degrees of alteration depending on the depth of the drill core sample, however, the type of alteration was fairly constant. All three samples analysed by petrography and EDS showed extensive sericite and chlorite alteration of the phenocrysts with sericitic alteration in the groundmass. Feldspar phenocrysts often

showed albitisation. Carbonate (dolomite, calcite, ankerite), muscovite, iron-oxide, tourmaline and minor epidote were also found in several of the samples.

5.3.1.2. Ealbara Rhyolite

The Ealbara Rhyolite was sampled in both the Gibralter 1 and Bulgunnia 2 drillholes, which are separated by 80km. Petrographical analysis revealed the Gibralter 1 samples were from a flow banded rhyolite which had broken and embayed phenocrysts (Figure 11e) indicating it was perhaps part of a higher energy eruption or a pyroclastic flow. The samples are heavily altered by sericite and clays. The Bulgunnia 2 samples showed Ealbara Rhyolite without flow banding and broken crystals highlighting the variation of textures within the unit. The samples appeared highly red coloured and sericite altered although the EDS analysis showed the groundmass composition was relatively unchanged, suggesting the hematite was too fine-grained or not abundant enough to change the composition. The EDS and thin section analysis showed many phenocrysts had been completely replaced by the assemblage quartz, albite, chlorite, carbonate $\pm$ clay.

5.3.1.3. Bittali Rhyolite

Bittali Rhyolite samples were collected from drillhole MSDP10 and outcrop locations. All of the MSDP10 samples showed significant sericite and chlorite alteration resulting in an overall pale green coloured rock. The petrology and EDS analysis of the 4 samples presented a mineral assemblage of sericite, chlorite, quartz and albite $\pm$ pyrite $\pm$ fluorite. Many of the feldspars had been altered to a chlorite, albite, potassium feldspar assemblage. Pyrite and lesser sphalerite and galena were found throughout with fluorite being associated with the pyrite (Figure 11b). Chlorite, pyrite, quartz and feldspar was

found to be spatially associated suggesting they formed by the same hydrothermal event. Comparatively, the outcrop sample thin section (2721824) analysed has a grey appearance and significantly less chlorite, no hematite and courser grain micas within the ground mass. The main alteration in this sample was sericite, iron-oxide and dolomite. This sample fits into the same category in Figure 10 but is considerably different than the MSDP10 samples.

5.3.1.4. Mangaroongah Dacite

One sample from the Mangaroongah Dacite displayed intense fine-grained hematite alteration of the groundmass with chlorite and iron-oxide (opaque) being the alteration products of many phenocrysts and also found within the groundmass.

5.3.1.5. Eucarro Rhyolite

Two Eucarro Rhyolite samples were chosen from the field as they resembled a highly silicified breccia outcrop consistent with epithermal style alteration. In thin section they displayed intense alteration of all phenocrysts with feldspars being altered completely to quartz and epidote and amphiboles being altered and partially destroyed by brown clay. The samples were brecciated and showed quartz veining with comb textures and vugs (Figures 3 & 11). Other hand samples that were chosen for geochemistry rather than the alteration study displayed hematite-sericite alteration that is common throughout the GRV outcrops.
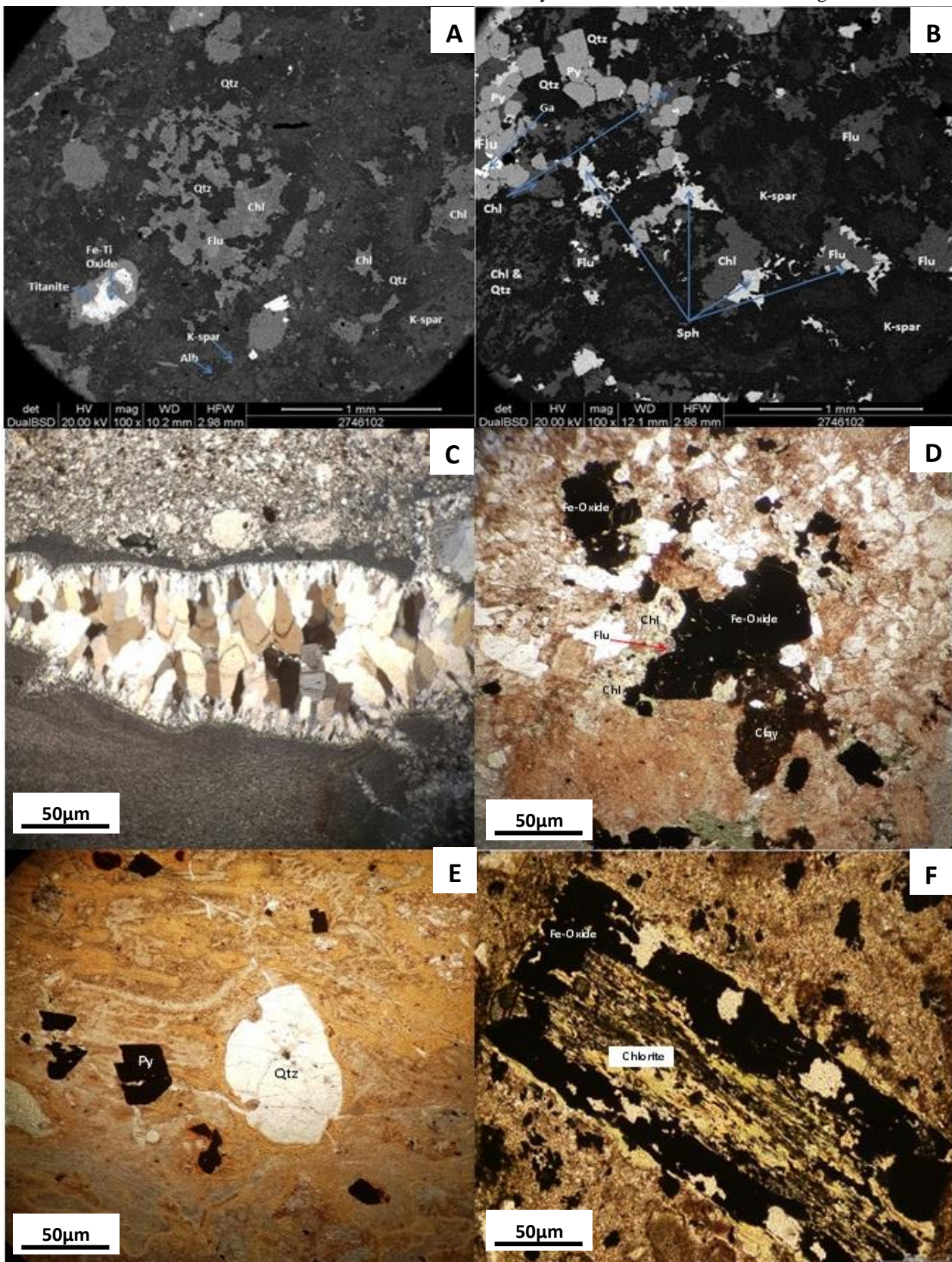
Figure 11: a) Electron Backscatter Image (EBI) showing qtz (quartz), chl (chlorite) and flu (fluorite) alteration assemblage within the Moonaree Dacite Member. b) EBI showing chl, flu, k-spar alteration and sph (sphalerite), py (pyrite), ga (galena) mineralisation within the MSDP10 Bittali Rhyolite. c) Comb quartz texture within Eucarro rhyolite silicified breccia sample. d) Fe-oxide, chl, flu and clay alteration within the Red 2 Dacite. e) Flowbanding around embayed qtz and secondary pyrite within the Ealbara Rhyolite. f) Previous mafic mineral altered to Fe-oxide and chlorite within the Moonaree Dacite Member.

5.3.1.6.   Moonaree Dacite Member

Three field samples from the Moonaree Dacite Member displayed pervasive

sericite/hematite alteration as well as pseudomorphs of phenocrysts which have been

altered to Fe-Ti-oxides, titanite, chlorite, quartz and albite which are spatially associated

(Figure 11a). One sample from the field displayed a grey colour which proved to be

almost unaltered with primary mafic minerals only partially altered.

6. DISCUSSION

6.1.   Magmatic evolution from lower to upper GRV.

The results of this work in conjunction with the recently published high precision dates

of GRV units (Jagodzinski et al., 2016) allow for a comparison of the changes in the

GRV magmatic system over a relatively short time span. In general, the lower GRV has

the most variable geochemistry with more dacitic and mafic (not studied here)

magmas present. It represents a 7 m.yr periodic emplacement of felsic to mafic

extrusive rocks that erupted in spatially and temporally distributed volcanic centres.

Throughout this time there were several successions of dacitic and rhyolitic units,

indicating an active mafic component replenishing the system. The upper GRV are

entirely felsic and most likely erupted from an evolved system (Giles, 1988; Stewart,

1994 unpublished). Recent Pb and Sm-Nd isotopic work on the GRV has indicated that

the upper and lower GRV magma systems either developed independently or evolved

significantly over a short (<2m.yr) time period (Chapman et al., 2019).

6.1.1. FRACTIONAL CRYSTALLISATION

Eu anomalies are variable in the GRV units. The lower GRV units showed variable Eu anomalies with the Bittali and Ealbara rhyolites having average Eu anomalies of 0.37 and 0.22 respectively and the Mangaroongah Dacite having an average Eu/Eu* value of 0.86 (Figure 7). This anomaly demonstrates the process of fractionation of plagioclase in which Eu^{2+} is taken up by plagioclase in place of Ca^{2+}. Plagioclase fractionation is further evidenced in the data by decreasing trends in Ca and Al (Figure 5). The larger negative Eu anomalies seen in some of the lower most felsic GRV units may indicate a larger degree of magma fractionation. The lower GRV Mangaroongah Dacite is relatively unfractionated (Eu/Eu* = 0.86). This contrast in Eu anomalies between volcanic centres highlights the developmental and heterogeneous nature of the lower GRV geochemical and magmatic evolution. It also evidences the interpretation that lower GRV volcanic centres developed separately. Mantle-like Pb-isotopic signatures have been found within the lower GRV in both mafic and felsic endmembers further suggesting magma evolution of the lower GRV was dominated by closed system processes such as fractional crystallisation (Chapman et al., 2019).

Upper GRV samples showed consistent Eu anomalies with the Eucarro Rhyolite and Moonaree Dacite Member having average Eu/Eu* values of 0.59 and 0.63 respectively (Figure 7). This consistency of Eu anomalies may reflect the maturity of the upper GRV system and that it was sourced by a single large magma chamber.

6.1.2. POSSIBLE MAFIC DRIVER IN THE MAGMATIC SYSTEM

As mentioned above, several dacitic units erupted shortly after rhyolite units in the lower GRV. This suggests there is a mafic component replenishing the lower GRV system, much of which is most likely un-erupted. This is also displayed in the upper GRV with the Moonaree Dacite Member being erupted after the Eucarro Rhyolite. Further evidence of a major mafic component within the upper GRV system is mafic enclaves found in the field within the Yardea Dacite and Eucarro Rhyolite (see Table 2 and Figure 3). They indicate an interaction of a mafic magma with the upper GRV felsic magma (Coombs et al., 2003). They also indicate active convection or turbulence within the magma chamber driven by the heat of an underlying basalt allowing mafic enclaves to be spread evenly through large portions of the upper GRV units (Bonin, 2004; Wiebe, 1994). The mafic enclaves are likely dispersed into the felsic magma by either turbulence at a mafic/felsic boundary within a stratified magma chamber or by direct injection of the mafic material into the felsic magma chamber (Frost et al., 1987; Wiebe, 1994). Either process implies a large amount of mafic magma within the upper GRV system that could have provided heat for melting, physically caused eruptions through displacement or chemically drove eruptions through addition of volatiles (Ferguson et al., 2019). As to why there is little other evidence of mafic material associated with the upper GRV, it may be due to the silicic melt trapping the basalt below (Wiebe, 1994).

6.1.3. MAGMATIC MODEL AND TECTONIC SETTING

Both upper and lower GRV data show possible large degrees of crustal contamination with highly enriched REE (Figure 9) and steep LREE/HREE (Figure 7) patterns ($(La/Sm)_N$ = 2.5 – 6.1). However, previous work on the GRV and Hiltaba Suite mafic and felsic rocks have shown that crustal contamination was minor in the lower GRV leading to a metasomatised/enriched sub-continental lithospheric mantle source for the lower GRV (Chapman, 2019; Stewart, 1994 unpublished; Wade, 2012). Variation seen in the lower GRV phase could be due to the system being in a developmental stage allowing volcanic centres to evolve separately, producing differing geochemistry. Consistency of negative Ba, Nb, Sr, Eu and Ti anomalies throughout upper/lower GRV suggests these characteristics are inherited from the source of the magma and not from a simple fractionation from a depleted mantle sourced basalt (Stewart, 1994 unpublished). This also indicates that the enriched SCLM source is the main source of both lower and upper GRV units and the significant change in magmatic evolution between the lower and upper GRV is not coincident with a large change in the source region.

A significant change in magmatic evolution between the upper and lower GRV (< 2 m.y) is theorised to have occured (Chapman et al., 2019; Stewart, 1994 unpublished). Evidence of this can be found in Figure 7 where $(La/Sm)_N$ values steadily decrease throughout the evolution of the lower GRV and suddenly rise with the onset of the upper GRV. Due to the volume of erupted magmas and homogeneity within the upper GRV units it is possible the upper GRV evolved as one or two large magma chambers. There is no known eruption centres found for the two main lava flows in the upper GRV, the Eucarro Rhyolite and Yardea Dacite. This means that the two successions

could have erupted hundreds of kilometers apart and therefore may have been sourced from separate magma chambers. The generation of these large felsic magma chambers may be the result of an amalgamation of the multiple magma chambers sourcing the lower GRV, creating a larger magma chamber or chambers. This process would also assimilate a larger amount of crust accounting for the increased crustal signature seen in the upper GRV (Chapman et al., 2019; Stewart, 1994 unpublished). The significant change in magmatic evolution in such a short time may suggest some external input mechanism contributed to this change. It was initially thought that the Gawler SLIP was emplaced in an anorogenic or broadly extensional setting (Flint et al 1993., Creaser et al., 1995). Early extension in the developmental stage of the GRV is evidenced by several syn-volcanic sedimentary units within the Roopena Basin (Curtis et al., 2018), at Olympic Dam (McPhie et al., 2011) and at Prominent Hill (Bull et al. 2015). However, evidence of syn-Gawler SLIP deformation in rock units proximal to the Gawler Craton and deformation associated with the Olarian and Kararan orogenies indicates that the tectonic stress regime switched to compression for some period of time during the emplacement of the Gawler SLIP (Hand, 2007; Hand, 2008; Wade et al., 2012). This contemporaneous high temperature metamorphism may have contributed to a larger degree of crustal melting and input into the system, as well as possibly assisting the amalgamation of the developmental plumbing system of the lower GRV. This switching of stress regimes in short periods of time could be due to a far-field subduction zone experiencing a period of slab rollback creating an extensional environment for the lower GRV (Skirrow et al., 2018; Wade et al., 2012) followed by convergence at the time of upper GRV emplacement.

6.2. Alteration in the GRV

6.2.1. STYLES OF ALTERATION

The results of the alteration analysis showed that while the main alteration type across the GRV is sericitic/phyllic there is still considerable variation from location to location and at different depths in the units when excluding the prevalent sericite alteration. There is variation in terms of both the alteration assemblages that have grown and also the intensity of alteration. It is apparent that there was a widespread alteration which had affected almost all of the outcropping GRV dominated by sericite and hematite. This alteration results in a red colour which is most common in the GRV. Some of the drillhole samples showed different types of alteration from the typical sericite–hematite alteration experienced by most of the outcropping samples. This could be the result of overprinting by a different episode of hydrothermal alteration or different fluid chemistry and volume due to variable basement lithologies and fluid focusing structures (faults, fractures, shear zones etc.). The widespread sericite – hematite alteration suggests the GRV was altered by one large hydrothermal event while variations in alteration resulted from other more localised hydrothermal systems. Intensity of alteration may have been affected by porosity of basement and GRV lithologies such as the volcanoclastic Ealbara Rhyolite encountered in the Gibralter 1 drillhole which showed evidence of fluid flow through the matrix. This increased fluid flow would affect the degree of alteration in surrounding lithologies as well as the porous unit itself. Although a limited number of Upper GRV samples were investigated during this analysis, field observations and rock descriptions have allowed for a general

understanding of widespread alteration in the upper GRV. The upper GRV Eucarro

Rhyolite displays sericite-hematite phyllic alteration which is common throughout the

GRV, while two silicified samples showed epithermal alteration characteristics. The

Moonaree Dacite Member shows sericite-hematite phyllic alteration with added

chlorite, most likely resultant of alteration of mafic minerals which are absent in the

rhyolite. Some samples of the Moonaree Dacite Member showed little to no hematite

alteration while all other samples from the other units showed some degree of sericite-

hematite alteration. This may be an important observation since the Moonaree Dacite

Member is the youngest of the recent TIMS dated GRV units and may indicate that the

widespread alteration event affecting the rest of the GRV may have finished at around

1587 Ma while the Moonaree Dacite Member was erupted. Further analysis of samples

from the upper GRV from different areas would be able to confirm this.

6.2.2. LINKING PETROGRAPHY AND EDS ANALYSIS WITH HYLOGGER™

6.2.2.1. Red 2 Dacite

The main alteration assemblage found within the Red 2 Dacite was sericite, chlorite,

iron-oxide ± carbonates ± epidote ± tourmaline. This alteration assemblage is supported

by the HyLogger™ data collected from the SARIG database for each sample depth. The

short-wave infra-red (SWIR) HyLogger data showed high percentages of

phengite/muscovite and chlorite as well as epidote in the deeper samples. The absence

of coarse grain muscovite or phengite in the thin sections suggests the high percentage

in the HyLogger™ data would be resulting from sericitic (fine mica alteration). Thermal

infra-red (TIR) HyLogger™ data was used in conjunction with the SWIR data and

confirmed the presence of sericite, chlorite and carbonates as well as revealing albite

and quartz undetectable by SWIR. The presence of dolomite and albite found in both the HyLogger[TM] data and the EDS/thin section analysis further suggests a phyllic alteration assemblage (Figure 10).

6.2.2.2. Ealbara Rhyolite

The Ealbara Rhyolite samples from the Gibralter 1 drillhole revealed heavy sericite/clay alteration. However, the alteration was so fine grained it wasn't clear on what type of clays were altering the rock. The SWIR HyLogger[TM] data was able to confirm the alteration assemblage, revealing that the rock had significant illite, smectite and phengite (sericite) as well as variable siderite. TIR data confirmed this and identified significant albite alteration, presumably of feldspar phenocrysts. The Bulgunnia 2 drillhole samples showed the alteration assemblage of sericite, hematite, quartz, albite, chlorite $\pm$ carbonate $\pm$ clay. Hylogger[TM] analysis of this drillhole was relatively inconclusive due to a high percentage of aspectral signature, however it did point out the presence of phengite (sericite), epidote, chlorite and carbonates (siderite, ankerite, calcite). No TIR data was available for this hole. Interestingly, the HyLogger[TM] data didn't show any hematite even though the thin section analysis showed it was present. This could be due to the small grain size of the hematite not producing enough of a signature for the HyLogger to detect.

6.2.2.3. Bittali Rhyolite

Bittali Rhyolite samples within the MSDP10 drillhole showed a phyllic alteration assemblage of sericite, chlorite, albite, quartz $\pm$ pyrite $\pm$ fluorite $\pm$ sphalerite $\pm$ galena. SWIR HyLogger[TM] data confirmed the presence of sericite in the form of muscovite and lesser phengite. It also confirmed the presence of chlorite of varying compositions (Fe,

Fe-Mg, Mg rich) and indicated the presence of tourmaline in all samples adding to the alteration assemblage. TIR data confirmed the sericitic alteration as muscovite as well as chlorite. It also revealed high percentages of quartz and feldspars related to the primary mineralogy.

6.2.3.   USEFULNESS OF HYLOGGER™ DATA TO REVEAL ALTERATION

From the four drillholes analysed using the HyLogger™ all showed significant alteration that was generally revealed by the data. It is apparent that the SWIR data was the most useful in being able to show a great deal of the alteration. This is because the SWIR detector is able to find minerals commonly associated with alteration, such as, micas, chlorites, carbonates, clays etc (Schodlok et al., 2016). The TIR data was also able to pick up some of these minerals but generally showed them as a small percentage (<5%), however, this still adds evidence that they are present within the rock. The TIR detector was most useful in being able to reveal quartz and different feldspars within the rock that were difficult to identify within the thin section analysis. Interpretation of these minerals is difficult however, as most of the quartz and feldspars are presumed to be part of the primary mineralogy of the rock while some may be resultant of alteration e.g. albitisation. The inability of the HyLogger™ to detect hematite alteration in any of the samples is of note considering previous work has indicated the presence of hematite within the sampled drillholes particularly the Gibralter 1 and Bulgunnia 2 drillholes. In order to check the validity of this observation HyLogger™ data for a hole located within the Prominent Hill deposit which is a well-known IOCG deposit with significant hematite alteration was analysed (Minotaur Exploration 2001). While the drillhole report for this hole stated there was a heavy presence of hematite alteration it was not detected by the HyLogger™. This inability to detect hematite may be due to the small

grain size of the hematite alteration. While this leads to a possible disadvantage of using the HyLogger^{TM} data to characterise alteration, the characteristic red rock alteration associated with hematite is obvious enough to disregard the HyLogger's^{TM} inability to identify the mineral. In general, when used in conjunction with core logging and further analysis like petrology and EDS; HyLogger^{TM} data is very useful in determining the overall alteration assemblage very quickly while also indicating the different compositions of some minerals such as chlorite and micas which may show some zonation of alteration that could be useful in exploration (Fabris et al., 2017).

6.2.4. ALTERATION ASSOCIATED WITH MINERALISATION

The lower GRV showed the largest variety of alteration perhaps due to the variable geochemical nature of the units themselves. Alteration types were mainly phyllic when taking the dominant sericite alteration into account, however, alteration minerals indicating propylitic and argillic alteration were also present in some samples (Table 3). This alteration that is divergent from the sericite - hematite alteration is much more likely to point to localised structures and systems such as orebodies. In the drillholes chosen for this study there was pyrite and uneconomic sulphide mineralisation present. The sulphides seemed to be associated with chlorite, quartz, iron-oxide $\pm$ fluorite alteration. This assemblage may represent another stage in hydrothermal alteration as geothermal activity continued for millions of years. While there are mineralogical similarities between the alteration described in this study and the typical phyllic alteration encountered in economic alteration systems (Sillitoe, 2010), the intensity is much lower; with hydrothermal breccias being more localised and primary mineralogical and textural characteristics being preserved quite well in most samples. The hydrothermal breccia encountered in the field within the Eucarro Rhyolite (upper

GRV) is interesting as it presents silicic alteration and mineral textures commonly associated with upper porphyry epithermal systems (Sillitoe, 2010; Wade, 2014). It is significant that epithermal systems may be found within the larger extent of the upper GRV since we now know that epithermal deposits have been preserved within the lower GRV and also often include outcropping silicic breccias.

7. CONCLUSIONS

1. Fractional crystallisation played a large part in the magmatic evolution of the GRV as evidenced by significant negative Eu anomalies, the largest of which are found within the lower GRV. The heterogeneous nature of Eu anomalies within the lower GRV is used as further evidence that the lower GRV volcanic centres evolved independently.

2. A large mafic component is thought to have driven the lower GRV and upper GRV. In the lower GRV component is directly evident in the mafic (basalt to andesite) volcanics that are exhibited in multiple lower GRV volcanic centres. In the upper GRV the mafic component is manifest as mafic enclaves found commonly in the upper GRV. Mafic magma in the upper GRV could have driven melting as well as eruption through volatile input and physical displacement.

3. Enrichments and depletions of trace elements are consistent with previously published literature and indicate an enriched mantle source with some degree of crustal input. Consistency of these enrichments/depletions is thought to reflect source characteristics of the GRV rather than magmatic processes occurring during the evolution of the magmas such as crustal assimilation. While a larger

degree of crustal input is expected within the upper GRV the consistencies mentioned above indicate that the primary source (enriched SCLM) remained constant throughout both lower and upper GRV emplacements.

4. The lower GRV is known to have evolved in several separate volcanic centres while the upper GRV is thought to have formed from one or two large magma chambers that were the result of an amalgamation of the lower GRV plumbing system. This explains the geochemically homogenous nature of the upper GRV as well as the increased crustal signature within the upper GRV. It is hypothesised that an external driver must have been needed to force the significant change of the GRV plumbing system is such a short time. The Olarian Orogeny and contemporaneous syn-Gawler SLIP deformation is suggested to have contributed to this process.

5. The alteration assessed in this study proved to have a major sericite – hematite component that was common to most of the samples analysed. This alteration is thought to represent a single continuous hydrothermal event. When discounting the sericite – hematite alteration it was found that the alteration was quite varied geographically most likely relating to fluid focusing structures and the effect of basement lithologies on hydrothermal fluid geochemistry.

6. The HyLogger[TM] was found to very useful in identifying alteration within drillholes that was otherwise difficult to identify in petrology and EDS; for example, sericitic alteration that was too fine grained to see in thin-section was evident in the HyLogger[TM] data. When used logically in addition to visual analysis such as petrology it proved very useful in identifying alteration assemblages.

7. Alteration associated with mineralisation was found within the four drillholes sampled during this analysis and it was found that sulphide mineralisation is associated with chlorite, quartz, iron-oxide ± carbonate ± fluorite alteration (phyllic). The discovery of epithermal style alteration and mineral textures within a hydrothermal breccia in the Eucarro Rhyolite is thought to be significant in that epithermal/porphyry systems have only been recognised within the lower GRV (and even those are relatively recent discoveries). This could indicate the possibility of porphyry/epithermal systems being preserved in the upper GRV which covers the majority of the outcropping GRV area, significantly extending the exploration search space for these systems.

8. ACKNOWLEDGMENTS

REFERENCES

AGANGI, A., KAMENETSKY, V. S., & MCPHIE, J. (2012). Evolution and emplacement of high fluorine rhyolites in the Mesoproterozoic Gawler silicic large igneous province, South Australia. *Precambrian Research, 208*, 124-144.

ALLEN, S., & MCPHIE, J. (2002). The Eucarro Rhyolite, Gawler Range Volcanics, South Australia: A> 675 km3, compositionally zoned lava of Mesoproterozoic age. *Geological Society of America Bulletin, 114*(12), 1592-1609.

ALLEN, S., MCPHIE, J., FERRIS, G., & SIMPSON, C. (2008). Evolution and architecture of a large felsic igneous province in western Laurentia: the 1.6 Ga Gawler Range Volcanics, South Australia. *Journal of Volcanology and Geothermal Research, 172*(1-2), 132-147.

ALLEN, S. R., SIMPSON, C. J., MCPHIE, J., & DALY, S. J. (2003). Stratigraphy, distribution and geochemistry of widespread felsic volcanic units in the Mesoproterozoic Gawler Range Volcanics, South Australia. *Australian Journal of Earth Sciences, 50*(1), 97-112. doi: 10.1046/j.1440-0952.2003.00980.x

BLISSETT, A. (1975). Rock units in the Gawler Range Volcanics, South Australia. *Geological Survey of South Australia Quarterly Geological Notes, 55*, 2-14.

BLISSETT, A. (1986). Subdivision of the Gawler Range Volcanics in the Gawler Ranges. *Geological Survey of South Australia Quarterly Geological Notes, 97*, 2-11.

BLISSETT, A.H., CREASER, R.A., DALY, S., FLINT, D.J., AND PARKER, A.J. (1993). Gawler Range Volcanics, in DREXEL, J.F., PREISS, W.V., AND PARKER, A.J., eds., The geology of South Australia. Vol 1. The Precambrian: South Australia Geological Survey, Bulletin 54, 107–131.

BONIN, B. (2004). Do coeval mafic and felsic magmas in post-collisional to within-plate regimes necessarily imply two contrasting, mantle and crustal, sources? A review. *Lithos, 78*(1-2), 1-24.

BRYAN, S. (2007). Silicic large igneous provinces. *Episodes, 30*(1), 20-31.

BRYAN, S., & FERRARI, L. (2013). Large igneous provinces and silicic large igneous provinces: Progress in our understanding over the last 25 years. *Geol. Soc. Am. Bull., 125*(7-8), 1053-1078. doi: 10.1130/B30820.1

BRYAN, S. E., & ERNST, R. E. (2008). Revised definition of large igneous provinces (LIPs). *Earth-Science Reviews, 86*(1-4), 175-202.

BULL, S., MEFFRE, S., ALLEN, M., FREEMAN, H., TOMKINSON, M., & WILLIAMS, P. (2015). Volcanosedimentary and chronostratigraphic architecture of the host rock succession at Prominent Hill, South Australia. SEG 2015: World-class ore deposits: Discovery to recovery, Hobart, Tasmanian Society of Economic Geologists, pp. abstract. Retrieved from http://www.segweb.org/SEG/_Events/Conference_Archives/2015/Conference_Proceedings/files/pdf /Oral-Presentations/Abstracts/Bull.pdf

CHAPMAN, N. D., FERGUSON, M., MEFFRE, S. J., STEPANOV, A., MAAS, R., & EHRIG, K. J. (2019). Pb-isotopic constraints on the source of A-type Suites: Insights from the Hiltaba Suite - Gawler Range Volcanics Magmatic Event, Gawler Craton, South Australia. *Lithos, 346-347*. doi: 10.1016/j.lithos.2019.105156

COOMBS, M. L., EICHELBERGER, J. C., & RUTHERFORD, M. J. (2003). Experimental and textural constraints on mafic enclave formation in volcanic rocks. *Journal of Volcanology and Geothermal Research, 119*(1-4), 125-144.

CREASER, R. A. (1995). Neodymium isotopic constraints for the origin of Mesoproterozoic felsic magmatism, Gawler Craton, South Australia. *Canadian Journal of Earth Sciences, 32*(4), 460-471.

CURTIS, S., & THIEL, S. (2019). Identifying lithospheric boundaries using magnetotellurics and Nd isotope geochemistry: An example from the Gawler Craton, Australia. *Precambrian Research, 320*, 403-423.

CURTIS, S., WADE, C., & REID, A. (2018). Sedimentary basin formation associated with a silicic large igneous province: stratigraphy and provenance of the Mesoproterozoic Roopena Basin, Gawler Range Volcanics. *Australian Journal of Earth Sciences, 65*(4), 447-463. doi: https://doi.org/10.1080/08120099.2018.1460398

CUTTS, K., HAND, M., & KELSEY, D. (2011). Evidence for early Mesoproterozoic (ca. 1590 Ma) ultrahigh-temperature metamorphism in southern Australia. *Lithos, 124*(1-2), 1-16.

DALY, S. (1998). Tectonic evolution and exploration potential of the Gawler Craton, South Australia. *AGSO J. Aust. Geol. Geophys., 17*, 145-168.

FABRIS, A., TYLKOWSKI, L., BRENNAN, J., FLINT, R., OGILVIE, A., CURTIS, S., . . . KEELING, J. (2017). Mineral Systems Drilling Program in the southern Gawler Ranges, South Australia. Report Book 2016/00030. *Department of the Premier and Cabinet, South Australia, Adelaide.* Retrieved from:

https://www.researchgate.net/publication/320014166_Mineral_Systems_Drilling_Program_in_the_southern_Gawler_Ranges_South_Australia/link/59c8799d0f7e9bd2c0147122/download

FAIRCLOUGH, M., (2005). Geological and metallogenic setting of the Carrapateena FeO-Cu-Au prospect—a PACE success story. *Minerals and Energy South Australia Journal*, 38, 4–7.

FANNING, C., FLINT, R., PARKER, A., LUDWIG, K., & BLISSETT, A. (1988). Refined Proterozoic evolution of the Gawler craton, South Australia, through U-Pb zircon geochronology. *Precambrian Research, 40*, 363-386.

FANNING, C., REID, A., & TEALE, G. (2007). A geochronological framework for the Gawler Craton, South Australia. *Bulletin* (Vol. 55): Primary Industries and Resources South Australia.

FERGUSON, M. R. M., EHRIG, K., MEFFRE, S., & FEIG, S. (2019). From magma to mush to lava: Crystal history of voluminous felsic lavas in the Gawler Range Volcanics, South Australia. *Lithos, 346*, 5148-5148.

FLINT, R. B., BLISSETT, A. H., CONOR, C. H. H., COWLEY, W. M., CROSS, K. C., CREASER, R. A., DALY, S. J., KRIEG, G. W., MAJOR, R. B., TEALE, G. S. AND PARKER, A. J., (1993). Mesoproterozoic. In: DREXEL, J. F., PREISS, W. V. AND PARKER, A. J. (Eds), The geology of South Australia; Volume 1, The Precambrian. *Geological Survey of South Australia,* Bulletin 54, 106-169. Retrieved from: https://sarigbasis.pir.sa.gov.au/WebtopEw/ws/samref/sarig1/image/DDD/BULL054(V1).pdf

FORBES, C. J., BETTS, P. G., WEINBERG, R., & BUICK, I. S. (2007). A structural metamorphic study of the Broken Hill Block, NSW, Australia: reply. *Journal of Metamorphic Geology, 25*(6), 719-723. doi: 10.1111/j.1525-1314.2007.00719.x

FRASER, G., MCAVANEY, S., NEUMANN, N., SZPUNAR, M., & REID, A. (2010). Discovery of early Mesoarchean crust in the eastern Gawler Craton, South Australia. *Precambrian Research, 179*(1-4), 1-21.

FRASER, G. L., SKIRROW, R. G., SCHMIDT-MUMM, A., & HOLM, O. (2007). Mesoproterozoic gold in the central Gawler craton, South Australia: geology, alteration, fluids, and timing. *Economic Geology, 102*(8), 1511-1539.

FRICKE, C., 2005. *Source and origin of the Lower Gawler Range Volcanics (GRV), South Australia: geochemical constraints from mafic magmas*. Monash University, Hons. thesis (unpublished).

FROST, T. P., & MAHOOD, G. A. (1987). Field, chemical, and physical constraints on mafic-felsic magma interaction in the Lamarck Granodiorite, Sierra Nevada, California. *Geological Society of America Bulletin, 99*(2), 272-291.

GARNER, A., & MCPHIE, J. (1999). Partially melted lithic megablocks in the Yardea Dacite, Gawler Range Volcanics, Australia: implications for eruption and emplacement mechanisms. *Bulletin of Volcanology, 61*(6), 396-410.

Geological Survey of South Australia's database SARIG (https://map.sarig.sa.gov.au/)

GILES, C. W., (1980). *A comparative study of Archaean and Proterozoic felsic volcanic associations in southern Australia*. University of Adelaide, PhD thesis (unpublished).

GILES, C. (1988). Petrogenesis of the Proterozoic Gawler Range Volcanics, South Australia. *Precambrian Research, 40*, 407-427.

HAND, M., REID, A., & JAGODZINSKI, L. (2007). Tectonic framework and evolution of the Gawler Craton, Southern Australia. *Economic Geology, 102*(8), 1377-1395.

HAND, M. P., REID, A. J., SZPUNAR, M. A., DIREEN, N., WADE, B., PAYNE, J., & BAROVICH, K. M. (2008). Crustal architecture during the early Mesoproterozoic Hiltaba-related mineralisation event: are the Gawler Range Volcanics a foreland basin fill? *MESA Journal, 51*, 19-24.

HEITHERSAY, P., (2002). Prominent Hill discovery—URN 1: The best copper-gold intersection in 25 years. *Minerals and Energy South Australia Journal*, 24, 4–5.

HOU, B., KEELING, J., REID, A., FAIRCLOUGH, M., WARLAND, I., BELOUSOVA, E., . . . HOCKING, R. (2011). Heavy mineral sands in the Eucla Basin, southern Australia: deposition and province-scale prospectivity. *Economic Geology, 106*(4), 687-712.

HUANG, Q., KAMENETSKY, V. S., EHRIG, K., MCPHIE, J., KAMENETSKY, M., CROSS, K., . . . DIREEN, N. G. (2016). Olivine-phyric basalt in the Mesoproterozoic Gawler silicic large igneous province, South Australia: Examples at the Olympic Dam Iron Oxide Cu–U–Au–Ag deposit and other localities. *Precambrian Research, 281*, 185-199.

JAGODZINSKI, E. (1985*). The Geology of the Gawler Range Volcanics in the Toondulya Bluff Area and U-Pb Dating of the Yardea Dacite at Lake Acraman* (Hons. Thesis). University of Adelaide, South Australia.

JAGODZINSKI, E., REID, A., CROWLEY, J., MCAVANEY, S., & WADE, C. (2016). *Precise Zircon U-Pb Dating of a Mesoproterozoic Silicic Large Igneous Province: The Gawler Range Volcanics and Benagerie Volcanic Suite, South Australia.* Paper presented at the Australian Earth Science Convention.

BAS, M., MAITRE, R., STRECKEISEN, A., & ZANETTIN, B. (1986). A Chemical Classification of Volcanic Rocks Based on the Total Alkali-Silica Diagram. *Journal of Petrology, 27*(3), 745-750.

MCPHIE, J., DELLAPASQUA, F., ALLEN, S., & LACKIE, M. (2008). Extreme effusive eruptions: Palaeoflow data on an extensive felsic lava in the Mesoproterozoic Gawler Range Volcanics. *Journal of Volcanology and Geothermal Research, 172*(1-2), 148-161.

MCPHIE, J., KAMENETSKY, V. S., CHAMBEFORT, I., EHRIG, K. AND GREEN, N. (2011). Origin of the supergiant Olympic Dam Cu-U-Au-Ag deposit, South Australia: was a sedimentary basin involved?. *Geology*, 39, 795-798. doi: https://doi.org/10.1130/G31952.1

NICOLSON, B., REID, A., MCAVANEY, S., KEELING, J., FRASER, G., & VASCONCELOS, P. (2017). Timing of advanced argillic alteration at Nankivel Hill, SE of Paris silver deposit, northern Eyre Peninsula.

PANKHURST, R., LEAT, P., SRUOGA, P., RAPELA, C., MÁRQUEZ, M., STOREY, B., & RILEY, T. (1998). The Chon Aike province of Patagonia and related rocks in West Antarctica: a silicic large igneous province. *Journal of Volcanology and Geothermal Research, 81*(1-2), 113-136.

PAUL, M. W., COOK, N. J., CIOBANU, C. L., ANDERSON, J., & MURRAY, J. (2015). Preliminary Mineralogical Investigations of the Paris Silver Deposit, Northern Eyre Peninsula, South Australia.

REID, A., HAND, M., JAGODZINSKI, E., KELSEY, D., & PEARSON, N. (2008). Paleoproterozoic orogenesis in the southeastern Gawler Craton, South Australia. *Australian Journal of Earth Sciences, 55*(4), 449-471.

REID, A. J., & HAND, M. (2012). Mesoarchean to mesoproterozoic evolution of the southern Gawler Craton, South Australia. *Episodes, 35*(1), 216-225.

REID, A. J., & PAYNE, J. L. (2017). Magmatic zircon Lu–Hf isotopic record of juvenile addition and crustal reworking in the Gawler Craton, Australia. *Lithos, 292-293*, 294-306. doi: 10.1016/j.lithos.2017.08.010

SCHODLOK, M., WHITBOURN, L., HUNTINGTON, J., MASON, P., GREEN, A., BERMAN, M., . . . JOLIVET, M. (2016). HyLogger-3, a visible to shortwave and thermal infrared reflectance spectrometer system for drill core logging: functional description. *Australian Journal of Earth Sciences, 63*(8), 929-940.

SILLITOE, R. H. (2010). Porphyry copper systems. *Economic Geology, 105*(1), 3-41.

SKIRROW, R., BASTRAKOV, E., BAROVICH, K., FRASER, G., FANNING, C., CREASER, R., & DAVIDSON, G. (2007). The Olympic Cu-Au province: timing of hydrothermal activity, sources of metals, and the role of magmatism. *Economic Geology, 102*, 1441-1470.

SKIRROW, R. G., WIELEN, S. E., CHAMPION, D. C., CZARNOTA, K., & THIEL, S. (2018). Lithospheric Architecture and Mantle Metasomatism Linked to Iron Oxide Cu- Au Ore Formation: Multidisciplinary Evidence from the Olympic Dam Region, South Australia. *Geochemistry, Geophysics, Geosystems, 19*(8), 2673-2705. doi: 10.1029/2018GC007561

STEWART, K., (1994). High temperature felsic volcanism and the role of mantle magmas in Proterozoic crustal growth: the Gawler Range volcanic province. University of Adelaide, PhD thesis (unpublished).

SUN, S.S., MCDONOUGH, W.F., (1989). Chemical and isotopic systematics of oceanic basalts; implications for mantle composition and processes. In: Saunders, A.D., Norry, M.J. (Eds.), Magmatism in the Ocean Basins. Geological Society Special Publications 42. Geological Society London, London, 313–345 https://doi.org/10.1144/GSL. SP.1989.042.01.19.

SWAIN, G., BAROVICH, K., HAND, M., & FERRIS, G. (2005). *Proterozoic magmatic arcs and oroclines: St Peter Suite, Gawler craton, South Australia.* Paper presented at the Supercontinents and Earth Evolution Symposium.

SWAIN, G., WOODHOUSE, A., HAND, M., BAROVICH, K., SCHWARZ, M., & FANNING, C. M. (2005). Provenance and tectonic development of the late Archaean Gawler Craton, Australia

TAYLOR, S.R., MCLENNAN, S.M., (1985). The Continental Crust: Its Composition and Evolution. Blackwell Scientific Publications, 312 https://doi.org/10.1002/gj.3350210116.

WADE, C. E., MCAVANEY, S. O., (2014). Epithermal-style textures, brecciation, veining and alteration, southern Gawler Ranges, South Australia (pp. pp. 35): Geological Survey of South Australia.

WADE, C. E., REID, A. J., WINGATE, M. T., JAGODZINSKI, E. A., & BAROVICH, K. (2012). Geochemistry and geochronology of the c. 1585 Ma Benagerie Volcanic Suite, southern Australia: Relationship to the Gawler Range Volcanics and implications for the petrogenesis of a Mesoproterozoic silicic large igneous province. *Precambrian Research, 206*, 17-35.

WIEBE, R. A. (1994). Silicic magma chambers as traps for basaltic magmas: the Cadillac Mountain intrusive complex, Mount Desert Island, Maine. *The Journal of Geology, 102*(4), 423-437.

APPENDIX A: GEOCHEMICAL DATA

Sample	Analysis	Unit	SiO2	Al2O3	Fe2O3	CaO	MgO	MnO	TiO2	SO3	P2O5	K2O	Na2O	BaO	LOI1000
UNITS	NA	NA	%	%	%	%	%	%	%	%	%	%	%	%	%
2721839	Geochem	Mangaroongah Dacite	64.91	14.58	5.42	1.14	2.07	0.145	0.922	0.018	0.35	4.65	3.8	0.256	1.67
2721825	Geochem	Bittali Rhyolite	74.49	13.24	2.15	0.13	0.18	0.17	0.144	0.025	0.029	5.03	3.36	0.074	0.91
2721824	Geochem	Bittali Rhyolite	74.16	13.03	2.26	0.07	0.06	0.095	0.274	0.017	0.028	5.9	2.64	0.077	0.95
884Bi5	Geochem	Bittali Rhyolite	72.65	13.2	1.55	1.54	0.34	0.05	0.2	0.015	0.059	5.4	3.04	0.06	1.92
884Bi2	Geochem	Bittali Rhyolite	73.65	14	1.19	0.19	0.1	-0.01	0.4	0.026	0.058	6	2.95	0.16	1.03
2746125	Geochem	Bittali Rhyolite	77.91	12.2	0.71	0.2	0.14	0.02	0.17	0.124	0.012	5.78	1.34	-0.01	1.09
2746129	Geochem	Bittali Rhyolite	79.54	9.45	1.5	0.13	0.3	0.05	0.12	1.12	0.014	4.96	1.48	-0.01	0.94
2721812	Geochem	Eucarro Rhyolite	73.18	13.16	2.13	0.34	0.11	0.08	0.415	0.23	0.057	5.59	3.2	0.536	1.11
2721816	Geochem	Eucarro Rhyolite	71.93	13.36	3.52	0.17	0.17	0.031	0.391	0.029	0.068	6.16	2.64	0.168	1.31
2721843	Geochem	Moonaree Dacite	66.1	13.62	5.38	0.47	1.98	0.047	0.764	0.031	0.211	8.21	1.52	0.177	1.18
2174053	Geochem	Moonaree Dacite	68.1	14.29	4.77	2.31	0.75	0.102	0.661	0.062	0.177	4.88	3.45	0.166	0.6
2174054	Geochem	Moonaree Dacite	70.26	13.6	4.05	1.75	0.45	0.101	0.531	0.033	0.124	5.09	3.32	0.143	0.34
2721818	Geochem	Moonaree Dacite	66.49	13.88	5.6	2.2	0.99	0.12	0.771	0.035	0.219	4.9	3.33	0.166	1.17
2721820	Geochem	Moonaree Dacite	66.61	13.84	5.67	1.93	1.25	0.136	0.801	0.052	0.226	4.86	3.19	0.152	1.32
2721826	Geochem	Moonaree Dacite	67.15	13.86	5.16	1.59	1.2	0.107	0.711	0.024	0.207	4.94	3.21	0.146	1.55
2721829	Geochem	Moonaree Dacite	68.54	13.81	4.4	0.86	1.3	0.089	0.603	0.028	0.15	5.42	3.24	0.16	1.3

2174047	Geochem	Moonaree Dacite	67.1	14.02	5.62	2.13	1.01	0.127	0.785	0.077	0.222	4.83	3.22	0.158	1.03
2721832	Geochem	Moonaree Dacite	66.3	14.08	5.51	2.32	1.02	0.119	0.782	0.019	0.22	4.72	3.31	0.179	1.17
R2729175	Geochem	Ealbara Rhyolite	75.78	12.19	2.49	0.07	0.15	0.026	0.172	0.015	0.02	6.25	2.23	0.034	0.56
R2729176	Geochem	Ealbara Rhyolite	75.06	12.46	1.76	0.33	0.23	0.139	0.18	0.046	0.019	5.63	2.81	0.031	0.85
R2729179	Geochem	Ealbara Rhyolite	76.07	12.44	1.77	0.25	0.35	0.041	0.173	0.045	0.019	5.54	2.56	0.029	0.76
R2729181	Geochem	Ealbara Rhyolite	70.16	13.88	3.02	0.68	1.07	0.1	0.543	0.02	0.161	5.85	3.2	0.11	1.43
R2729182	Geochem	Ealbara Rhyolite	77.64	12.07	1.15	0.27	0.1	0.024	0.165	0.016	0.008	4.94	3.47	0.008	0.38
R2729184	Geochem	Red 2 Dacite	67.86	14.49	5.12	0.51	0.93	0.042	0.712	0.021	0.168	6.37	2.58	0.12	1.27
R2729186	Geochem	Red 2 Dacite	67.93	14.79	4.53	0.91	0.91	0.051	0.718	0.095	0.162	5.6	3.25	0.123	1.18
R2729188	Geochem	Red 2 Dacite	67.38	14.57	4.67	0.81	0.99	0.061	0.747	0.128	0.177	6.14	2.84	0.123	1.2
R2729189	Geochem	Red 2 Dacite	64.73	14.41	6.32	1	1.33	0.069	0.823	0.325	0.272	6.79	2.75	0.145	1.4
R2729190	Geochem	Red 2 Dacite	64.67	14.32	6.31	1.48	1.23	0.056	0.867	0.623	0.283	7.36	2.34	0.154	1.15
R2729191	Geochem	Red 2 Dacite	67.54	14.1	4.53	1.44	1.16	0.039	0.68	0.221	0.212	6.02	2.98	0.119	1.12
R2729177	Alteration	Ealbara Rhyolite	74.69	12.56	1.96	0.38	0.35	0.077	0.168	0.034	0.019	6.12	2.76	0.037	0.89
R2729178	Alteration	Ealbara Rhyolite	75.97	12.49	1.71	0.24	0.21	0.041	0.174	0.138	0.02	5.76	2.79	0.032	0.6
R2729183	Alteration	Ealbara Rhyolite	64.73	18.29	1.76	0.4	0.32	0.114	0.195	0.094	0.005	6.4	6.6	0.03	0.82
R2729185	Alteration	Red 2 Dacite	68.49	11.32	10.72	0.44	1.93	0.197	0.538	0.013	0.126	1.21	0.42	0.001	2.41
R2729187	Alteration	Red 2 Dacite	57.78	9.53	17.26	2.73	3.17	0.638	0.476	0.013	0.109	1.15	0.04	0.002	6.76
R2729187 Rpt	Alteration	Red 2 Dacite	57.58	9.5	17.18	2.77	3.18	0.639	0.468	0.015	0.11	1.14	0.05	0.001	6.71
2721821	Alteration	Eucarro Rhyolite	89.94	6.01	0.56	0.05	0.05	0.003	0.22	0.018	0.029	1.49	0.05	0.034	1.42
2721822	Alteration	Eucarro Rhyolite	90.44	4.57	1.56	0.2	0.06	0.004	0.109	0.044	0.031	1.47	0.05	0.042	1.36

Sample	Analysis	Unit	Ag	As	Ba	Be	Bi	Cd	Ce	Co	Cr	Cs	Cu	Dy	Er	Eu	Ga
UNITS	NA	NA	ppm	ppm	ppm	ppm	ppm	ppm	ppm	ppm	ppm	ppm	ppm	ppm	ppm	ppm	ppm

2721839	Geochem	Mangaroongah Dacite	0.1	1.4	2360	3	0.08	0.1	132	24.5	11	4.91	8	8.63	4.9	3.17	20.6
2721825	Geochem	Bittali Rhyolite	0.2	0.4	663	3.4	0.22	-0.1	114	35.7	9	1.08	4	3.97	2.06	0.94	18.7
2721824	Geochem	Bittali Rhyolite	-0.1	0.6	698	3	0.16	0.2	262	16.6	8	1.75	16	10.2	5.46	1.45	24
884Bi5	Geochem	Bittali Rhyolite	-0.1	1	646	2.6	0.04	-0.1	145	77.8	4	1.09	4	4.05	1.92	1.27	18.4
884Bi2	Geochem	Bittali Rhyolite	-0.1	0.2	1440	2.8	0.04	-0.1	397	64.6	-1	2.64	6	16.5	9.01	4.1	25
2746125	Geochem	Bittali Rhyolite	-0.1	11.2	97.5	3.8	0.04	-0.1	151	30.2	3	6.16	-2	9.45	5.73	0.47	19.5
2746129	Geochem	Bittali Rhyolite	0.2	22.2	84.5	5.2	0.04	2.3	122	49.7	2	2.19	4	8.85	4.55	0.4	13.5
2721812	Geochem	Eucarro Rhyolite	0.2	3.2	5090	3.4	0.18	0.4	173	21	7	1.05	6	10.5	6.24	2.31	23.5
2721816	Geochem	Eucarro Rhyolite	-0.1	1.4	1490	2.8	0.12	-0.1	105	12.4	7	3.93	18	10.5	6.6	1.73	24.5
2721843	Geochem	Moonaree Dacite	-0.1	2.4	1610	4	0.1	-0.1	152	22.3	10	3.3	6	10.2	6.16	2.43	21.5
2174053	Geochem	Moonaree Dacite	0.1	2	1560	3.4	0.16	0.3	154	22.4	7	2.94	8	9.39	5.43	2.4	22.4
2174054	Geochem	Moonaree Dacite	-0.1	2	1280	3.8	0.2	0.2	166	17.3	8	2.99	8	10.6	6.06	2.3	23.1
2721818	Geochem	Moonaree Dacite	-0.1	1	1560	3.6	0.28	0.4	161	19	14	2.77	14	10.2	6	2.57	21.7
2721820	Geochem	Moonaree Dacite	0.1	2.2	1420	3.6	0.12	0.5	162	18.7	12	2.87	12	10.6	6.27	2.5	22.3
2721826	Geochem	Moonaree Dacite	0.1	2.4	1370	4	0.1	0.2	152	13.5	7	3.03	14	9.69	5.79	2.37	22.4
2721829	Geochem	Moonaree Dacite	-0.1	1.8	1470	3.8	0.14	0.2	155	14.7	8	3.47	8	9.59	5.71	2.15	22.7
2174047	Geochem	Moonaree Dacite	-0.1	2.2	1420	3.4	0.18	0.2	156	18.8	8	3.49	14	9.97	6.1	2.46	22.6
2721832	Geochem	Moonaree Dacite	0.1	2	1610	3.2	0.12	0.1	152	18.1	8	3.66	26	9.55	5.67	2.39	22.9
R2729175	Geochem	Ealbara Rhyolite	-0.1	0.6	279	2.6	0.08	0.4	257	23.8	3	3.83	20	10.8	6.05	0.81	20.1
R2729176	Geochem	Ealbara Rhyolite	-0.1	0.6	252	3.4	0.06	-0.1	189	23.2	4	2.38	4	9.99	6.07	0.6	22.4
R2729179	Geochem	Ealbara Rhyolite	0.2	0.2	244	2.8	0.1	0.1	189	22	3	3.1	16	9.86	6.22	0.58	21.2

R2729181	Geochem	Ealbara Rhyolite	0.1	1.8	964	5.6	0.34	0.1	127	24.9	14	2.7	22	7.32	4.6	1.51	23.2
R2729182	Geochem	Ealbara Rhyolite	0.1	7.4	55.5	4.6	0.42	-0.1	93.2	29.4	4	1.95	4	6.13	4.34	0.29	22.3
R2729184	Geochem	Red 2 Dacite	0.1	7.8	1060	4.6	2.08	0.1	224	26.9	9	2.68	44	11.4	6.91	2.92	19.8
R2729186	Geochem	Red 2 Dacite	0.3	5.8	1080	3.8	0.42	0.1	197	25.3	9	1.48	78	11.5	7.28	2.79	20.8
R2729188	Geochem	Red 2 Dacite	0.1	4.8	1120	3.8	0.22	-0.1	185	30.4	2	1.72	226	10.6	6.39	2.66	21
R2729189	Geochem	Red 2 Dacite	0.1	1.8	1300	3.8	0.14	-0.1	205	27.8	5	1.02	146	10.2	5.71	2.49	20.3
R2729190	Geochem	Red 2 Dacite	0.2	2.8	1380	2.2	0.1	-0.1	218	40.9	4	1.2	108	10.2	6	3.17	18.9
R2729191	Geochem	Red 2 Dacite	2.8	2.4	1040	4	0.12	0.1	172	24.1	11	1.28	64	10.1	6.13	2.42	20.4
R2729177	Alteration	Ealbara Rhyolite	0.2	0.8	277	3.4	1.5	-0.1	192	21	5	4.51	4	10.4	6.41	0.59	18.2
R2729178	Alteration	Ealbara Rhyolite	0.1	0.8	249	4	0.16	0.1	191	27	1	3.56	18	10	6.51	0.62	22.7
R2729183	Alteration	Ealbara Rhyolite	-0.1	10.2	204	7	0.28	-0.1	132	13.5	3	1.27	4	8.14	5.9	0.39	42.2
R2729185	Alteration	Red 2 Dacite	0.4	7.6	36.5	4.2	0.9	-0.1	257	57.9	5	0.52	28	7.82	4.41	3.75	26.7
R2729187	Alteration	Red 2 Dacite	-0.1	7.2	47.5	3.6	0.28	-0.1	79.1	85.1	7	0.57	34	5.49	3.27	1.19	15.9
R2729187 Rpt	Alteration	Red 2 Dacite	0.1	6.4	49	3.6	0.34	-0.1	80.6	84	4	0.61	32	5.66	3.36	1.26	15.6
2721821	Alteration	Eucarro Rhyolite	0.2	6.6	322	2.8	0.12	0.1	116	17.1	4	3.78	8	5.59	3.55	0.9	11
2721822	Alteration	Eucarro Rhyolite	0.2	19	422	1.8	0.34	0.2	61.9	18.9	5	3.95	26	4.5	2.62	0.54	8.9

Sample	Analysis	Unit	Gd	Ge	Hf	Ho	In	La	Lu	Mn	Mo	Nb	Nd	Ni	Pb	Pr	Rb
UNITS	NA	NA	ppm	ppm	ppm	ppm	ppm	ppm	ppm	ppm	ppm	ppm	ppm	ppm	ppm	ppm	ppm
2721839	Geochem	Mangaroongah Dacite	10.1	1.2	10.5	1.76	0.05	64.1	0.63	1250	0.4	15.9	62.3	14	20	16	143
2721825	Geochem	Bittali Rhyolite	5.17	0.95	4.61	0.76	-0.05	58.8	0.24	1430	1	14.9	41.7	6	15	12.7	177
2721824	Geochem	Bittali Rhyolite	12.1	1.25	12	1.98	0.1	114	0.77	822	0.6	23	94.7	4	23	27.6	239
884Bi5	Geochem	Bittali Rhyolite	6.3	0.9	4.99	0.75	-0.05	74.3	0.24	441	1.2	11.2	55.1	4	23	16.5	154
884Bi2	Geochem	Bittali Rhyolite	22.1	1.2	13.8	3.31	0.1	203	1.2	19	1.8	25.4	163	-2	42	45.6	245
2746125	Geochem	Bittali Rhyolite	10.5	0.8	7.2	2.06	-0.05	74.6	0.8	200	1.6	22.8	65.2	-2	25	18.2	327
2746129	Geochem	Bittali Rhyolite	9.92	0.85	5.4	1.74	-0.05	61.6	0.56	358	10	17.4	53.9	-2	158	15.2	217

2721812	Geochem	Eucarro Rhyolite	10.9	1.3	12	2.21	0.1	88.9	0.89	649	1.6	24.7	70.4	10	81	19.6	243
2721816	Geochem	Eucarro Rhyolite	8.39	1.35	14.4	2.23	0.1	49.8	0.98	247	3	27	42.9	10	20	11.7	292
2721843	Geochem	Moonaree Dacite	10.8	1.3	11.5	2.08	0.05	76.6	0.84	384	1.2	20.6	65.5	14	20	17.2	238
2174053	Geochem	Moonaree Dacite	9.99	1.25	11.4	2.01	0.1	80	0.79	861	1.8	21.1	63.5	10	37	17.6	214
2174054	Geochem	Moonaree Dacite	11.3	1.25	11	2.13	0.1	84.4	0.88	864	2.4	23	69.4	6	40	18.7	233
2721818	Geochem	Moonaree Dacite	10.9	1.25	11.2	2.09	0.05	82.4	0.86	1030	1.6	21	67.4	14	31	18.4	212
2721820	Geochem	Moonaree Dacite	11.5	1.3	11.7	2.14	0.05	84.2	0.87	1150	2.4	21.7	69.8	14	37	18.8	207
2721826	Geochem	Moonaree Dacite	10.6	1.3	11	2.02	0.1	78.6	0.79	888	0.8	20.3	64.7	8	36	17.5	208
2721829	Geochem	Moonaree Dacite	9.94	1.4	11.9	1.97	0.1	80.7	0.84	748	0.6	21.1	63.1	6	6	17.4	236
2174047	Geochem	Moonaree Dacite	10.5	1.25	11.8	2.05	0.1	80.5	0.89	1030	2	20.4	65.9	8	37	17.9	202
2721832	Geochem	Moonaree Dacite	10.6	1.25	11.1	2	0.1	78	0.77	975	1.2	19.9	63.6	8	35	17.2	205
R2729175	Geochem	Ealbara Rhyolite	14.6	0.9	9.73	2.15	0.05	148	0.86	209	0.6	23.4	103	4	36	28.5	266
R2729176	Geochem	Ealbara Rhyolite	10.4	1	10.1	2.09	0.1	97.5	0.93	1110	1	24.2	74.9	4	18	21.3	249
R2729179	Geochem	Ealbara Rhyolite	10.4	0.95	9.9	2.05	0.1	97.6	0.89	321	3.6	23.7	74.3	6	34	21.1	249
R2729181	Geochem	Ealbara Rhyolite	7.93	1.35	10.1	1.48	0.1	70.4	0.69	816	0.4	21	54.5	16	63	15.6	242
R2729182	Geochem	Ealbara Rhyolite	5.75	1.3	7.59	1.39	0.05	44	0.72	180	0.2	26.9	31.2	4	45	9.7	261
R2729184	Geochem	Red 2 Dacite	12.8	1.35	12	2.36	0.1	121	0.92	341	1	26.9	86.1	8	6	24.7	295
R2729186	Geochem	Red 2 Dacite	12.5	1.15	12.1	2.42	0.05	105	1.03	403	2	26.6	78.4	12	12	22	251
R2729188	Geochem	Red 2 Dacite	11.8	1.15	11.9	2.15	0.05	98.3	0.93	507	1.4	27	74.3	4	24	20.6	263
R2729189	Geochem	Red 2 Dacite	11.2	1.05	10	2.14	-0.05	121	0.81	558	4	23.1	73.8	4	10	21.7	283
R2729190	Geochem	Red 2 Dacite	11.4	1.25	10	2.16	-0.05	129	0.83	459	2.2	22.7	77.3	6	26	22.8	303
R2729191	Geochem	Red 2 Dacite	10.9	1.35	9.9	2.06	-0.05	92.9	0.85	318	2.8	21.3	67.5	10	22	19.2	249
R2729177	Alteration	Ealbara Rhyolite	11	0.8	9.36	2.23	0.1	99.6	0.91	610	0.6	23.8	76.4	-2	38	21.4	246
R2729178	Alteration	Ealbara Rhyolite	10.9	1.05	9.9	2.15	0.1	101	0.95	335	0.8	24.7	75.9	4	28	21.3	253
R2729183	Alteration	Ealbara Rhyolite	6.82	0.75	11	1.87	0.1	63.6	1.08	940	0.2	34.5	41.5	4	45	12.9	215
R2729185	Alteration	Red 2 Dacite	11.8	1.85	8.86	1.49	0.25	162	0.67	1660	1.6	19.5	93.3	12	5	27.3	74.6
R2729187	Alteration	Red 2 Dacite	5.33	1.45	7.47	1.16	0.55	48.6	0.56	5360	0.8	17.3	30	8	3	8.51	96.5

R2729187 Rpt	Alteration	Red 2 Dacite	5.47	1.5	7.58	1.21	0.55	51.3	0.52	5380	0.8	17.1	31.5	10	3	8.69	92.6
2721821	Alteration	Eucarro Rhyolite	5.37	1.3	7.17	1.2	0.05	59.4	0.49	21	12.4	13.8	42.9	4	36	12.5	83.1
2721822	Alteration	Eucarro Rhyolite	4.22	1.3	4.66	0.92	0.05	32.9	0.38	31	13	9.05	23.8	4	40	6.67	67.5

Sample	Analysis	Unit	Re	Sb	Sc	Se	Sm	Sn	Sr	Ta	Tb	Te	Th	Ti	Tl	Tm	U
UNITS	NA	NA	ppm	ppm	ppm	ppm	ppm	ppm	ppm	ppm	ppm	ppm	ppm	ppm	ppm	ppm	ppm
2721839	Geochem	Mangaroongah Dacite	-0.01	0.4	15.8	-5	12.5	2.4	325	1	1.53	-0.2	14.9	6050	0.6	0.69	2.6
2721825	Geochem	Bittali Rhyolite	0.02	-0.1	3.1	-5	8.31	2	131	1.14	0.78	-0.2	33.4	911	0.8	0.3	5.67
2721824	Geochem	Bittali Rhyolite	0.02	0.2	7	-5	17.3	3.8	31.2	1.51	1.86	-0.2	31.4	1750	1	0.81	6.28
884Bi5	Geochem	Bittali Rhyolite	0.02	-0.1	3.7	-5	9.68	2	174	1.05	0.83	-0.2	26.8	1260	1.4	0.28	4.48
884Bi2	Geochem	Bittali Rhyolite	0.03	0.2	7.9	-5	28.4	4.4	94	2.03	3.08	-0.2	35.8	2450	1.6	1.3	7.37
2746125	Geochem	Bittali Rhyolite	0.02	0.6	2.5	-5	12.6	5.2	20.6	1.72	1.66	-0.2	34.8	1050	2	0.85	7.06
2746129	Geochem	Bittali Rhyolite	0.01	0.5	2.9	-5	11.4	2.4	22.4	1.36	1.61	-0.2	26.6	813	1.6	0.63	5.74
2721812	Geochem	Eucarro Rhyolite	-0.01	0.2	8.8	-5	13.2	4	141	1.82	1.75	-0.2	37.9	2610	1	0.93	8.25
2721816	Geochem	Eucarro Rhyolite	-0.01	0.2	8	-5	9.28	4.4	117	1.92	1.63	-0.2	34.5	2460	1.6	1.02	7.55
2721843	Geochem	Moonaree Dacite	-0.01	0.2	12.1	-5	12.8	3.4	131	1.41	1.71	-0.2	27	4940	0.8	0.87	3.74
2174053	Geochem	Moonaree Dacite	-0.01	0.2	10.8	-5	12.1	4.2	217	1.58	1.63	-0.2	27.8	4220	0.8	0.82	5.82
2174054	Geochem	Moonaree Dacite	-0.01	0.2	10.4	-5	13.4	4.2	162	1.67	1.78	-0.2	29.6	3410	1	0.9	6.13
2721818	Geochem	Moonaree Dacite	-0.01	0.2	13.1	-5	13	3.4	195	1.4	1.74	-0.2	27.4	5030	0.8	0.89	5.78
2721820	Geochem	Moonaree Dacite	-0.01	0.2	13.2	-5	13.5	3.6	207	1.5	1.82	-0.2	28.1	5130	0.8	0.93	5.75
2721826	Geochem	Moonaree Dacite	-0.01	0.3	12.2	-5	12.4	4	181	1.46	1.66	-0.2	27.7	4620	1.2	0.86	5.77
2721829	Geochem	Moonaree Dacite	-0.01	0.3	9.7	-5	11.8	3.8	129	1.52	1.64	-0.2	30.1	3910	1.2	0.85	6.43
2174047	Geochem	Moonaree Dacite	-0.01	0.1	12.3	-5	12.8	3.8	249	1.45	1.68	-0.2	26.7	4960	1	0.86	5.52
2721832	Geochem	Moonaree Dacite	-0.01	0.2	12.1	-5	12.6	3.6	230	1.46	1.63	-0.2	25.7	4840	1.2	0.83	5.54
R2729175	Geochem	Ealbara Rhyolite	-0.01	0.3	4.6	-5	18.1	3.2	55.9	1.56	1.99	-0.2	28.1	1070	1.8	0.91	6
R2729176	Geochem	Ealbara Rhyolite	-0.01	0.2	4.4	-5	13.7	4	60.7	1.64	1.64	-0.2	28.7	1100	1.4	0.88	5.69
R2729179	Geochem	Ealbara Rhyolite	-0.01	0.2	4.3	-5	13.9	3.4	52.1	1.62	1.74	-0.2	28.7	1120	1.2	0.92	5.87

Sample	Analysis	Unit														
R2729181	Geochem	Ealbara Rhyolite	-0.01	0.3	7.9	-5	10.4	3.2	106	1.5	1.26	-0.2	26.7	3380	0.8	0.69	8.24
R2729182	Geochem	Ealbara Rhyolite	-0.01	0.6	2.4	-5	6.67	3.8	13.3	1.86	1.03	-0.2	34.3	999	1.2	0.68	6.73
R2729184	Geochem	Red 2 Dacite	-0.01	0.7	11.7	-5	16.4	4	68	2.05	2	1.2	42.9	4530	0.4	1.01	6.93
R2729186	Geochem	Red 2 Dacite	-0.01	0.4	11.9	-5	14.9	4.8	106	2.15	1.99	0.2	43.6	4670	0.2	1.08	11.2
R2729188	Geochem	Red 2 Dacite	0.02	0.4	11.6	-5	14.2	4.6	102	2.19	1.84	-0.2	42.6	4830	0.4	0.97	11.7
R2729189	Geochem	Red 2 Dacite	0.04	0.2	12.6	-5	13.5	7.4	96.4	1.94	1.74	-0.2	38.2	5340	0.2	0.84	13.3
R2729190	Geochem	Red 2 Dacite	0.02	0.2	14.4	-5	13.8	7.8	122	1.98	1.73	-0.2	37.7	5630	0.2	0.87	12.2
R2729191	Geochem	Red 2 Dacite	0.01	0.3	11.1	-5	12.8	6.4	132	1.65	1.7	-0.2	38.8	4330	0.2	0.9	12
R2729177	Alteration	Ealbara Rhyolite	-0.01	0.2	4.5	-5	14.1	4.2	58.3	1.63	1.69	-0.2	28.6	1040	1.4	0.97	6.11
R2729178	Alteration	Ealbara Rhyolite	-0.01	0.2	4.4	-5	14	4.6	58.8	1.72	1.67	-0.2	29.8	1080	1.2	0.94	8.34
R2729183	Alteration	Ealbara Rhyolite	0.01	0.4	4.1	-5	8.02	4.4	30.6	2.28	1.29	-0.2	49.1	1210	1	0.92	7.37
R2729185	Alteration	Red 2 Dacite	-0.01	0.9	13	-5	16.6	15.8	33.9	1.56	1.48	0.6	28.5	3460	-0.2	0.67	6.23
R2729187	Alteration	Red 2 Dacite	-0.01	1	8.2	-5	6.06	4	7.7	1.35	0.94	0.2	25.6	2960	-0.2	0.48	8.1
R2729187 Rpt	Alteration	Red 2 Dacite	0.01	1.2	8.4	-5	6	3.8	7.9	1.32	0.96	-0.2	25.3	2950	-0.2	0.5	8.22
2721821	Alteration	Eucarro Rhyolite	-0.01	9.9	4.1	-5	7.52	1.4	20.8	0.94	0.9	-0.2	18.1	1390	0.2	0.54	4.72
2721822	Alteration	Eucarro Rhyolite	0.02	10.8	2.6	-5	4.81	1.6	26.9	0.67	0.76	-0.2	13	696	0.2	0.39	2.89

Sample	Analysis	Unit	V	W	Y	Yb	Zn	Zr	AU1	AU2	Pt	Pd	F	FeO
UNITS	NA	NA	ppm	ppm	ppm	ppm	ppm	ppm	ppb	ppb	ppb	ppb	%	%
2721839	Geochem	Mangaroongah Dacite	74.8	89	44.6	4.29	115	416	5	NA	-1	-1	0.08	1.99
2721825	Geochem	Bittali Rhyolite	6	262	21.3	1.73	30	139	3	NA	-1	-1	0.07	0.11
2721824	Geochem	Bittali Rhyolite	2.1	110	52	5.14	110	440	6	NA	-1	-1	0.09	-0.1
884Bi5	Geochem	Bittali Rhyolite	15.3	759	19.2	1.7	80	167	24	21	-1	-1	0.065	0.43
884Bi2	Geochem	Bittali Rhyolite	3.7	537	84.7	7.9	25	522	8	6	-1	-1	0.095	0.12
2746125	Geochem	Bittali Rhyolite	0.5	234	53.4	5.46	20	206	16	NA	-1	-1	0.03	0.15
2746129	Geochem	Bittali Rhyolite	0.5	344	43.3	3.71	300	150	30	NA	-1	-1	0.065	0.63
2721812	Geochem	Eucarro Rhyolite	4.6	152	58	6.04	80	430	5	NA	-1	-1	0.09	-0.1

2721816	Geochem	Eucarro Rhyolite	6.2	84.5	56.2	6.42	85	540	5	NA	-1	-1	0.07	0.46
2721843	Geochem	Moonaree Dacite	35.2	93.5	56.4	5.56	50	420	11	NA	-1	-1	0.15	0.87
2174053	Geochem	Moonaree Dacite	27.9	126	51.8	5.31	90	437	5	NA	-1	-1	0.13	3.1
2174054	Geochem	Moonaree Dacite	14.4	105	56.2	5.85	100	392	4	NA	-1	-1	0.13	2.21
2721818	Geochem	Moonaree Dacite	36.6	88	56.6	5.63	100	426	5	NA	-1	-1	0.12	3.43
2721820	Geochem	Moonaree Dacite	38.8	88.5	56.8	5.78	105	431	5	NA	-1	-1	0.12	3.55
2721826	Geochem	Moonaree Dacite	33.8	52	53.8	5.63	100	401	4	NA	-1	-1	0.11	2.61
2721829	Geochem	Moonaree Dacite	24.2	79.5	52.7	5.51	100	443	4	NA	-1	-1	0.12	2.5
2174047	Geochem	Moonaree Dacite	36.3	93	53.9	5.67	100	431	4	NA	-1	-1	0.12	3.47
2721832	Geochem	Moonaree Dacite	37.6	88.5	51.9	5.36	100	413	4	NA	-1	-1	0.12	3.21
R2729175	Geochem	Ealbara Rhyolite	2.8	186	56	5.77	65	320	4	NA	-1	-1	0.04	0.15
R2729176	Geochem	Ealbara Rhyolite	3.1	176	55.9	5.95	40	329	13	NA	1	3	0.18	0.44
R2729179	Geochem	Ealbara Rhyolite	2.4	174	55.5	5.94	50	324	12	NA	-1	2	0.07	0.34
R2729181	Geochem	Ealbara Rhyolite	18.9	175	41.9	4.77	180	353	7	NA	-1	-1	0.09	0.58
R2729182	Geochem	Ealbara Rhyolite	1.6	233	41	4.7	50	196	5	NA	-1	-1	0.17	0.18
R2729184	Geochem	Red 2 Dacite	28.6	140	61.9	6.43	30	429	6	NA	-1	1	0.11	1.85
R2729186	Geochem	Red 2 Dacite	26.4	140	62.5	6.94	40	438	7	NA	-1	-1	0.05	1.77
R2729188	Geochem	Red 2 Dacite	27.7	142	55.2	6.07	45	431	10	NA	-1	-1	0.09	1.85
R2729189	Geochem	Red 2 Dacite	50.1	130	53.6	5.26	40	364	6	NA	-1	-1	0.23	2.47
R2729190	Geochem	Red 2 Dacite	55	158	53.8	5.69	30	349	34	NA	-1	-1	0.17	2.71
R2729191	Geochem	Red 2 Dacite	38	143	54.6	5.67	40	354	6	NA	-1	1	0.18	1.9
R2729177	Alteration	Ealbara Rhyolite	3.7	169	60.8	6.13	75	312	5	NA	-1	-1	0.04	0.28
R2729178	Alteration	Ealbara Rhyolite	2.6	207	56.2	6.18	65	324	6	NA	-1	1	0.05	0.29
R2729183	Alteration	Ealbara Rhyolite	3.5	87.5	54.8	6.57	85	282	4	NA	-1	-1	0.02	0.26
R2729185	Alteration	Red 2 Dacite	30.7	183	40.2	4.13	90	331	42	43	-1	-1	0.15	6.31
R2729187	Alteration	Red 2 Dacite	17.8	81	30.1	3.46	240	289	9	NA	-1	-1	0.09	13.1
R2729187 Rpt	Alteration	Red 2 Dacite	17.3	81.5	30.7	3.47	240	279	12	NA	1	1	0.08	12.9

| 2721821 | Alteration | Eucarro Rhyolite | 2.9 | 160 | 31.5 | 3.32 | 15 | 272 | 5 | NA | -1 | -1 | 0.04 | -0.1 |
| 2721822 | Alteration | Eucarro Rhyolite | 2.7 | 173 | 25.1 | 2.44 | 15 | 165 | 5 | NA | 1 | -1 | 0.03 | 0.1 |

APPENDIX B: THIN SECTION DESCRIPTIONS

Sample	Unit	Modal Abundances		Description
		Phenocrysts	**Groundmass**	
2729189	**Red 2 Dacite**	**Phenocrysts: 50%** Alkali Feldspar – 30% Plagioclase – 50% Quartz – 15% Pyrite – 2% Chlorite – 1% Fe Oxide opaque – 1% Dolomite – 1% Fluorite - <1%	**Groundmass: 50%** Alkali Feldspar – 40% Quartz – 40% Plagioclase – 20%	Crystalline groundmass of quartz, alkali feldspar and plagioclase represents 50% of the volume at around 0.5-1mm in size. Plagioclase and alkali feldspar (up to 10mm) are the dominant phenocrysts and display anhedral to euhedral grain shapes. Perthitic feldspar textures are common and multiple twinning in plagioclase is observed where alteration is less intense. Feldspars are variably altered to sericite and hematite with sericite being more closely associated with plagioclase while hematite is more prevalent in the alkali feldspar grains. Pyrite is common and is associated with dark aggregates of iron oxide and chlorite. Other common alteration minerals include chlorite, iron oxide (opaque), dolomite and minor fluorite. These minerals represent an assemblage that are spatially associated and form aggregates.
2729187	**Red 2 Dacite**	**Phenocrysts: 30%** Quartz – 40% Feldspars – 40% Mafics – 20%	**Groundmass: 70%** Quartz – 60% Feldspars – 30%	Crystalline groundmass of quartz 80% and alkali feldspar 20% is pervasively altered by green mineral (Illite or sericite?) and hematite. There are distinct zones of hematite alteration and zones of dark green alteration. There is a late stage 3mm vein comprised of quartz which is

			Dolomite – 10%	un-altered. Feldspar and perhaps mafic phenocrysts (up to 4mm) are completely altered by green chlorite and illite/sericite. Needle shaped specular hematite is prevalent in some zones associated with the patches of chlorite/illite. While iron oxide is anhedral throughout the rest of the sample. Rutile is common as an accessory phase. Iron oxides are found throughout.
2729185	Red 2 Dacite	Phenocrysts: 20% Altered feldspars – 50% Quartz – 50%	Groundmass: 80% Quartz – 70% Muscovite – 15% Blue tourmaline – 15%	Cryptocrystaline groundmass dominated by anhedral quartz and altered by hematite with overgrowths of needle shaped sericite and amorphous sericite and rutile associated with Fe oxide opaque mineral. Feldspars are completely altered to iron oxide and muscovite. Groundmass is variably altered by sericite and iron oxide. Convolute up to 1cm layers of dark green alteration minerals are present and are comprised of cloudy chlorite and phenocrysts of strongly pleochroic blue tourmaline separated by layers of un-altered quartz.
2729183	Bulgunnia 2 – Ealbara Rhyolite	Phenocrysts: 25% Alkali Feldspar – 80% Psuedomorphs containing K-feldspar, Opaque, Chlorite ± Rutile– 20%	Groundmass – 75% Alkali feldspar – 50% Plagioclase – 50%	Porphyritic rhyolite with a cryptocrystalline groundmass of alkali feldspar and albite. Sub-hedral to euhedral alkali felspars are the dominant phenocrysts (<3mm) and commonly display perthitic textures and simple twinning. The other main phenocrysts are pseudomorphs (<2mm) most likely after mafic minerals, containing felspar, quartz, iron-oxide, chlorite, dolomite ± halite. This assemblage has completely psuedomophed the previous mineral leaving little evidence of what it was, although it presents a sub-hedral tabular grain shape. The K-feldspar is moderately altered to sericite and iron-oxide (hematite). The entire groundmass has been altered by hematite which is concentrated in microfractures and small patches throughout the rock.
2729182	Bulgunnia 2 – Ealbara Rhyolite	Phenocrysts – 80% Plagioclase – 90% Quartz – 10%	Groundmass – 20% Quartz – 30% Feldspars – 70%	Porphorytic rhyolite with a cryptocrystalline groundmass of variable grainsize consisting of euhedral to sub-hedral plagioclase, quartz and k-feldspar. The phenocrysts are highly variable in size ranging from 0.5mm to 5mm. Plagioclase is the dominant phenocryst and are euhedral – sub-hedral and displays multiple twinning, is inclusion rich and displays occasional embayment. The groundmass is highly altered

				by hematite making it hard to see primary mineral characteristics however many of the groundmass quartz displays a simplectic texture with the hematitie altered mineral.
2729180	**Gibralter 1** **Ealbara Rhyolite**	**Phenocrysts: 35%** Quartz – 35% Feldspathoid aggregates – 35% Plagioclase – 20% Pyrite – 10%	**Groundmass: 65%** Quartz – 50% Feldspars – 50%	Porphyritic, flow banded rhyolite with convolute layers of very fine grain feldspars and larger grain quartz. Feldspar phenocrysts displays euhedral to anhedral, angular shape sometimes forming aggregates of broken phenocrysts that the flow banding deforms around. Quartz shows broken angular phenocrysts as well as rounded embayed textures. Euhedral pyrite is found throughout the sample. Randomly oriented fractures cross-cut all phenocrysts and groundmass. The entire groundmass is heavily altered by clays.
2729178	**Gibralter 1** **Ealbara Rhyolite**	**Phenocrysts: 40%** Quartz – 50% Feldspars – 50%	**Groundmass: 60%** Quartz/feldspar – 100%	Porphyritic, flow banded rhyolite with convolute layers of very fine grain quartz/feldspar matrix. Quartz s up to 4mm and displays rounded embayed textures. Feldspars are up to 6mm, sub-hedral, are albitised and display perthitic twinning. Feldspars are altered by hematite and chlorite. The chlorite is found mainly within the feldspars but also in fractures within the matrix and displays a pale green colour with low pleochroism. Iron oxide and minor fluorite are also found within many of the altered feldspars. The ground mass is heavily altered by hematite creating a brick red colour.
2746122	**MSDP 10 Bittali** **Rhyolite**	**Phenocrysts: 20%** Plagioclase – 40% Potassium feldspar – 30% Quartz – 20% Hornblende – 5% Opaque – 1%	**Groundmass: 80%** Quartz – 80% K – Feldspar – 20%	Porphyritic rhyolite with a cryptocrytsaline groundmass of mainly quartz and k-feldspar. Phenocrysts are euhedral to sub-hedral with the dominant phenocryst being plagioclase followed by k-feldspar and then quartz and rare amphibole of grain size up to 4mm. The plagioclase phenocrysts show variable chloritoid and sericite alteration and are often completely destroyed. K-feldspar is altered mainly by sericite and chloritoid. Feldspars are often altered to albite, orthoclase and chloritoid. Quartz is sub-rounded and generally un-altered. The groundmass is altered by sericite and chloritoid. A common alteration assemblage is chloritoid, pyrite, iron-oxide, fluorite and chloritoid. Fluorite is associated with pyrite often found within the pyrite grain.

2746123	**MSDP 10 Bittali** **Rhyolite**	**Phenocrysts: 15%** Quartz – 50% K-feldspar – 25% Plagioclase – 25%	**Groundmass: 85%** Quartz – 50% Feldspars – 40% Vesicles – 10%	Porphyritic rhyolite with cryptocrystalline quartz-feldspar groundmass and vesicular texture. Quartz is sub-rounded and unaltered. Plagioclase is altered by chloritoid and sericite. K-feldspars are altered by sericite to a lesser extent. Vesicles are partially to fully infilled by quartz. The groundmass is altered by sericite. A common alteration mineral assemblage is chloritoid, iron-oxide, ± pyrite, ± flourite, ± tourmaline.
2746126	**MSDP 10 Bittali** **Rhyolite**	**Phenocrysts: 40%** Quartz – 70% K-feldspar – 20% Plagioclase – 5% Pyrite – 5%	**Groundmass: 60%** Quartz/Feldspar – 100%	Porphyritic rhyolite with cryptocrtalline matrix comprised mainly of quartz and k-feldspar. Phenocrysts are mainly sub-rounded quartz which is unaltered and commonly embayed. K-feldspar phenocrysts are albitised and sericitized. Groundmass is flow banded and altered by sericite. Plagioclase is less common and is altered by sericite. Quarts rich layers are courser grain and host the mineral assemblage of qtz, chloritoid, pyrite, ± fluorite ± sphalerite ± galena.
2746127	**MSDP 10 Bittali** **Rhyolite**	**Phenocrysts: 50%** Quartz – 60% K feldspar – 30% Plagioclase – 10%	**Groundmass: 50%** Quartz/Feldspar – 100%	Rhyolite with cryptocrytaline groundmass comprised of mainly quartz. Phenocrysts are quartz k-feldspar and plagioclase. Quartz is sub-rounded and displayed broken and embayed textures. K-felspar is albatised and sericitized and is sub-hedral to euhedral. Quartz-pyrite veins are common. The groundmass is flow banded and altered by sericite and clay minerals. Trace fluorite is present in some of the quartz veins. The common alteration assemblage is sericite, pyrite, brown clay mineral ± fluorite.
2721832	**Moonaree** **Dacite Member**	**Phenocrysts: 70%** Plagioclase – 55% K-feldspar – 40% Mafics – 5%	**Groundmass: 30%** K-feldspar – 40% Quartz – 30% Plagioclase – 30%	Cryptocrystalline groundmass comprised of quartz and felspars and are generally anhedral to subhedral. Plagioclase is the dominant phenocryst showing multiple twinning and euhedral grain shapes. K – felspar phenocrysts are often albitised and all feldspars are altered by hematite/sericite alteration. Previously mafic phenocrysts have often been altered to chlorite. The groundmass is pervasively altered by hematite. Chlorite, epidote, titanite and Ti-oxide have also grown as a result of alteration and are commonly spatially associated. Apatite is common as an accessory phase.

2721821	Silicified sample – Eucarro Rhyolite	Phenocrysts: 10% Quartz – 80% Altered feldspars – 20%	Groundmass – 90% Quartz – 90% Feldspar – 10%	Silicified porphyritic rhyolite with cryptocrystalline groundmass. Phenocrysts are mostly sub-rounded quartz, up to 2mm in size that displays embayed textures. Previous feldspar phenocrysts up to 1mm are altered completely to quartz and epidote. Fluorite is found throughout in small proportions and inside altered grains. The groundmass is altered by silicic minerals and rutile. There is a quartz vein that shows comb quartz textures and recrystalised silified alteration extending into the sample from the vein.
2721822	Silicified sample – Eucarro Rhyolite			Same as 2721821. Less fluorite.
2721824	Bittali Rhyolite	Phenocrysts – 40% Plagioclase- 40% K-feldspar – 40% Quartz – 20%	Groundmass: 60% Quartz/feldspar 100%	Porphyritic rhyolite with cryptocrystalline groundmass. The main phenocrysts are plagioclase and k-feldspar which show euhedral grain shapes up to 5mm in size. The quartz phenocrysts are up to 3mm and show rounded embayed textures. The plagioclase phenocrysts show albitisation and irregular multiple twinning. K-feldspar displays perthitic and simple twinning. Felspars are altered by sericite with patches of dolomite and iron oxide. The groundmass is pervasively altered by a needle shaped feldspar and iron oxide.
2174053	Moonaree Dacite Member	Phenocrysts: 60% Plagioclase - 70% Clinopyroxene – 12% Orthopyroxene – 8% Iron oxide – 10%	Groundmass: 40% Feldspar/quartz – 100%	Porphyritic dacite with a cryptocrystalline groundmass. Feldspars are the dominant phenocryst with plagioclase being the most prevalent feldspar. Feldspars are altered by a sericite. Pyroxenes are common and display high birefringence and pleochroism. Clinopyroxene is dominant over orthopyroxene. The groundmass is comprised of a feldspar/quartz matrix and is altered by sericite and chlorite with a small amount of biotite. The pyroxenes are partially altered and rimmed by chlorite.

2721825	**Moonaree** **Dacite Member**	**Phenocrysts: 60%** Quartz – 70% Plagioclase – 20% Chlorite – 10%	**Groundmass:** Quartz/feldspar – 100%	Mafic minerals are completely altered to actinolite or chlorite and iron oxide and same high relief mineral 2721839. Yellow and green slightly pleochroic mineral with moderate relief and high birefringence (Epidote) is commonly altering feldspars.
2721829	**Moonaree** **Dacite Member**	**Phenocrysts: 50%** Plagioclase – 50% K-feldspar – 40% Quartz – 10%	**Groundmass:** **50%** Quartz/feldspar 100%	Porphyritic dacite with a cryptocrystalline groundmass featuring a needle shaped colourless mineral. The main phenocrysts are plagioclase and k-feldspar which are subhedral. The plagioclase displays multiple twinning where less altered and the k-feldspar displays albitisation textures. The feldspars have been variably altered by hematite and chlorite. The groundmass has been heavily altered by hematite and lesser chlorite. Mafic minerals have been completely replaced by chlorite, brown clay and fluorite. Alteration minerals include hematite, chlorite, clay, fluorite.
2721839	**Mangaroongah** **Dacite**	**Phenocrysts: 10%** Plagioclase – 70% K-feldspar – 150% Quartz – 10% Chlorite – 5%	**Groundmass:** **90%** Quartz/feldspar – 100%	Porphyritic dacite with cryptocrystalline groundmass. Low phenocryst percentage with plagioclase being the dominant phenocryst. The feldspars show sub-rounded and embayed to euhedral textures and are up to 4mm. Quartz shows rounded an embayed textures up to 2mm. Feldspars are altered by hematite and lesser chlorite. Previous mafic minerals have been completely altered to chlorite, iron oxide and epidote. The groundmass is heavily altered by hematite, chlorite and iron oxide.

APPENDIX C: PETROGRAPHY/EDS RESULTS

Red 2 Dacite:
2729189: Chlorite, iron-oxide, dolomite ± fluorite ± pyrite. **HyLogger:** Phengite, Chlorite, epidote, carbonates
Phyllic - Propylitic
2729187: Mafic psuedomorphs - Dark green intense turbid Chlorite, **matrix** - dolomite ± rutile **HyLogger:** Phengite, Chlorite, Carbonates, albite
Phyllic
2729185: Chlorite, Tourmaline, sericite, iron oxide **HyLogger:** Phengite(Sericite), Chlorite, albite, dolomite, Tourmaline
Phyllic

Bulgunnia 2: Ealbarra Rhyolite
2729183: **Mafic psuedomorphs** - Chlorite, iron oxide, Ti-oxide, sericite, dolomite,
Matrix – sericite/muscovite, iron oxide, hematite **HyLogger:** Phengite, epidote
Phyllic – Outer-propylitic
2729182: Hematite, sericite
Phyllic

Gibralter 1: Ealbarra Rhyolite
2729180: Clays, pyrite **HyLogger:** Phengite, phengite-illite, smectite, pyrophyllite
Sericitic - Argillic
2729178: hematite, chlorite, iron-oxide, hematite (groundmass) ± fluorite **HyLogger:** Phengite, illite, siderite, albite
Sericitic - Argillic

MSDP 10: Bittali Rhyolite
2746122: Sericite, albite, chlorite, pyrite, iron-oxide, fluorite. **HyLogger:** Musc, Phengite, chlorite, tourmaline
Sericitic - Phyllic
2746123: Sericite, chlorite, iron oxide, ± pyrite ± fluorite ± tourmaline **HyLogger:** Musc, Phengite, chlorite, tourmaline
Sericitic - Phyllic

2746126: Sericite, albite, chlorite, pyrite ± fluorite ± sphalerite ± galena **HyLogger:** Musc, illite, chlorite
Sericitic - Phyllic
2746127: Sericite, albite, brown clay, ± fluorite **HyLogger:** Musc, Phengite, chlorite, tourmaline
Sericitic - Phyllic

Field sample - Eucarro Rhyolite
2721821 – silicified sample –Sericite, Quartz, rutile, ± fluorite
Silicic
2721822 – Same as 2721821 with less fluorite.
silicic

Field sample - Bittali Rhyolite
2721824 – sericite, iron-oxide (opaque), dolomite, albite
Sericitic - phyllic

Field sample – Moonaree Dacite
2174053 – sericite, chlorite
Sericitic - Phyllic
2721825 – hematite, epidote, chlorite, iron-oxide,
Outer propylititc
2721829: hematite, chlorite, brown clay
Hematitic
2721832: Sericite, hematite, albite, epidote, titanate, Ti-oxide.
Phyllic-propylititc

Field sample - Mangaroongah Dacite
2721839 – hematite, chlorite, iron-oxide,

APPENDIX D: FIELD OBSERVATIONS

Stop	Sample	Longitude	Latitude	Rock unit	Description
1	2721812	136.7684445	-32.619493	Eucarro Rhyolite	Porphyritic rhyolite with 10-40% phenocrysts of mostly euhedral feldspars and some sub-rounded quartz. Phenocrysts are 1-10mm in size. Phenocryst percentage and size varies over a meter scale. Groundmass is fine grain. Rock is altered to a red brown colour.
2	2721813	136.7757597	-32.55596585	Eucarro Rhyolite	Porphyritic rhyolite with 30-40% phenocrysts of mostly euhedral feldspars and some sub-rounded quartz. Phenocrysts are 1-10mm in size. Plagioclase appears zoned or altered by k-feldspar. Phenocryst percentage and size varies over a meter scale. Groundmass is fine grain. Rock is altered to a red brown colour. Mafic enclaves up to 50mm found
3	2721814, 2721815	136.7673264	-32.55998743	Eucarro Rhyolite	Same as stop 2 including mafic enclaves.
4	2721816	136.7091667	-32.54756797	Eucarro Rhyolite	Porphyritic red/brown rhyolite with smaller phenocryst size than last stop (up to 5mm). Outcrop is columnar jointed.
5	2721817	136.2611449	-32.49429527	Moonaree Dacite Member	Red/brown porphyritic dacite with 30-40% phenocrysts of mostly euhedral plag and lesser k-feldspar (5-20mm). 2mm rounded phenocrysts of grey quartz is common. Dark green glomerocrysts or previously mafic monerals are common and up to 5mm in size. Groundmass is crptocrystaline.
6	2721818	136.2713107	-32.48125172	Moonaree Dacite Member	Same rock type as stop 5. Feldspar pheonocrysts make up 30% of rock volume. Less dark green minerals than stop 5. Many large feldpars have been altered to k-feld, plag and quartz. Occasional sub-rounded large (40mm) quartz pheoncrysts. Outcrop is columner jointed. Mafic enclaves up to 70mm present.

7	2721819 2721820	136.305086	-32.45377048	Moonaree Dacite Member	Same rock type as stop 6 with less phenocrysts. Pheonocrysts are generally smaller than stop 6 but plag up to 20mm is common. K-feld up to 5mm. Dark green mineral up to 10mm. Dark green mineral has inclusions of feldspar. Large up to 100mm mafic enclaves present and a sample of one was taken.
8	2721821 2721822	136.3290427	-32.50608828	Eucarro Rhyolite	Porphyritic rhyolite with 10% phenocryst volume of mostly quartz (up to 3mm) and lesser sub-hedral feldspar. Quartz veining and silicification is prevalent. There is a 5m wide outcrop of slicious breccia. Vugs with quartz infill are common. Veins are quarts mixed with chalcedony.
9	2721823	136.278001	-32.5590561	Eucarro Rhyolite	Porphyritic rhyolite similar to stop 2 with feldspars representing 30% of rock volume and typically 3-5mm in size. Phenocrysts are mostly plag (60%), K-feldspar (30%) and mafic mineral (10%) with little to no quartz.
10	2721824	136.3483565	-32.65632145	Bittali Rhyolite	Porphyritic rhyolite with up to 15% vol of up to 5mm feldspars. Fresh rock is light grey in colour. Groundmass is crystalline made of round quartz and infilling feldspar. Phenocrysts of quartz are commonly round. Some minerals have been altered to epidote.
11	2721825	136.3536773	-32.67168547	Bittali Rhyolite	Porphyritic rhyolite with 20 vol of phenocrysts of rounded quartz (2-4mm) and lesser feldspars (K-feldspar being dominant over plagioclase). Very fine grain matrix. Rock is red/brown colour and quite different to stop 10.
12	2721826	136.1272161	-32.42013835	Moonaree Dacite Member	Red/brown porphyritic dacite with 70% phenocrysts and 30% fine grain semi-crystaline groundmass. Phenocrysts are plag – 40%, K-feld – 20%, 30% mafic mineral and 10% quartz. Feldspars with quartz centres common and up to 20mm.

13	2721827	136.1332768	-32.42315865	Moonaree Dacite Member	Only 200m East of stop 12 and is the same rock type with similar modal abundances.
14	2721828	136.1049922	-32.37301775	Moonaree Dacite Member	Same rock type as stop 12 with less phenocrysts. 2mm quartz phenocrysts with feldspar rims are still common. Quartz is variable with some areas with 10%vol quartz and areas with no quartz.
15	2721829	136.1034117	-32.41513158	Moonaree Dacite Member	Same rock type as stop 12 with 50% phenocrysts. 1-5mm feldspars and quartz is more common. Coronal feldspars around quarts up to 25mm in size is common.
17	2721831	135.7924322	-32.17112578	Moonaree Dacite Member	Same rock type as stop 12. Red/brown dacite with 40% phenocryst percentage. Phenocrysts are 45% plag, 35% mafic mineral, 20% k-feld. Mafic mineral often includes plagioclase.
18	2721832-2721836	135.6554845	-32.19878755	Moonaree Dacite Member	Same rock type as stop 12 with 70% phenocryst percentage. Plagiclase, k-feldspar and mafic mineral are similar in abundance and commonly 1-5mm with up to 20mm feldspars occasional. Mafic enclaves are common. Samples 192721833, 2721835 and 2721836 are mafic enclave samples
19	2721837	135.2056954	-31.788411	Mym1 Andesite	Andesitic member of the Mangaroongah dacite within the Glyde Hill Volcanic complex. Dark red/grey porphyritic andesite with 15-20% phenocrysts of mostly red altered plagioclase (5-15mm). Feldspars are sub-hedral with lesser euhedral phenocrysts. Feldspars are often zoned with dark mineral inclusions. Mafic phenocrysts up to 5mm are common. 7mm grey quartz is rare. Hydrothermal quartz veining up to 40mm wide forming a 1m brecciated zone.
20	2721838 2721839 2721840	135.2056954	-31.788411	Mangaroongah Dacite	Dark Red/brown porphyritic dacite with 15-20% phenocrysts of subhedral plag and k-feld. Up to 5mm quartz crystals common. Flowbanding is present and often folded and truncated. There are

					areas that seem less consolidated and include clasts. Possible pyroclastic deposit.
21	2721841	135.5640049	-31.7346101	Moonaree Dacite Member	Red/brown phenocryst rich dacite (70% phenocrysts). Phenocrysts are 40 plag, 40% mafic mineral, 20% k-feld. Feldspars are 2-4mm and mafic minerals are 0.5-2mm. Matrix is semicrystalline.
22	2721842	135.6828177	-31.81549747	Moonaree Dacite Member	Same rock type as stop 21 with less phenocrysts. Similar modal abundances.
23	2721843	135.851831	-31.98724195	Moonaree Dacite Member	Same rock type as stop 21 with 50% phenocrysts. Fresh surface is more dare grey/red. K-feld is more dominant over plagioclase. Groundmass is more crystalline and quartz rich.

APPENDIX E: FULL METHODS

Choosing samples:
Field rock samples were collected based on several parameters. A good geographical spread of samples was required and so sample sites areas were chosen before the trip and while on the trip. Units that had been recently dated by Jagodzinski were also chosen so geochemical analysis could be compared to an accurate timeline and attributed to the exact sites that the rocks were dated. Areas that had not been sampled yet were also chosen to improve the geographical spread of the data. Outcrops and rock samples were chosen on the basis that they were in situ and as unweathered as possible which was checked by hitting them with a hammer. Rocks were described at each site and the site was rehabilitated after each sample was taken to ensure there was as little impact as possible.
Drillholes were also chosen based on several factors. Red 2 was chosen because it contained LGRV that had been dated and so the geochemistry was able to be compared temporally to other samples that had been dated. Red 2, Gibralter 1, Bulgunnia 2 and MSDP10 were also chosen as they contained LGRV that had been altered and mineralised in different ways which would provide a good range of geochemistry and petrology of different alteration associated with the GRV. Bulgunnia 2 and Gibralter 1 contained Ealbara Rhyolite and MSDP10 contained the Bittali Rhyolite which are units that have been accurately dated making these holes even more useful for this analysis. Less altered samples were chosen for whole rock geochemistry for the geochemical analysis while different alteration types were identified and sampled to for the alteration study. Basic logs and observations of alteration were also made.
Petrology:
Petrological samples were taken from the field and from drill core for the purpose of creating thin sections for the alteration analysis. Thin section blocks were cut and sent to Adelaide Petrographic Laboratories to be made into thin sections. Thin sections were then viewed using a Leica microscope and described and characterised according to alteration minerals and style.

Rock Saw:
In order to reduce rock samples from the field to manageable sizes for the Jaw Crusher the samples had to be cut using the rock saw while some very large samples had to be broken with a sledgehammer first.
1. Wash off the saw and stage to remove any material from previous runs.
2. Place rock onto stage and turn on the saw. Ensure water is running onto the blade
3. Make cuts to remove any weathered rind from the sampled and cut the remainder into smaller sizes (3 X 5 X 10cm maximum) while cutting a small block for thin sections.
4. Remove samples and wash off the mud and dry on hot plates.
5. Wash debris off the rock saw and stage between each sample.

Jaw Crusher:
1. Clean the benches and floor to ensure minimal contamination.

2. Clean Jaw Crusher
   2.1 Unlock the door and open up the machine.
   2.2 Open the jaw plates and blow it with compressed air to remove loose dust and chips
   2.3 Use wire brush to loosen stuck on dust and blow it off again.
   2.4 Use ethanol to wipe away any remaining dust from any of the surfaces that touch the samples and use air to evaporate the ethanol.
3. Clean catch tray with ethanol and air hose and place butchers paper into tray before inserting into crusher.
4. Close up machine and turn it on.
5. Drop pieces of sample one at a time into crusher ensuring to quickly close the top hatch after every drop to stop any rocks being thrown out of the machine.
6. After the entire sample is crushed, turn off the crusher and open the machine and take out the catch tray.
7. Split the sample using a clean ruler or similar to take a small amount for milling ensuring to avoid bias by taking different sized fragments representing the ratio of the overall crushed sample.
8. Bag the crushate and repeat steps 2 – 5.

Vibrating Ring Mill:
1. Clean milling room.
2. Clean the tungsten mill rings and components using ethanol twice to ensure no residue will contaminate the sample.
   2.1 Squirt ethanol onto mill head components and wipe with paper towel then dry with compressed air.
   2.2 Repeat ensuring to only place components onto clean butchers' paper and then back into the mill pot once clean.
   2.3 If powder is caked onto components, then the mill will have to be run with pure quartz to remove residue and then cleaned using the above steps.
3. Evenly distribute the aliquoted crushate between the components of the mill head.
4. Place mill head into machine and secure with clamp.
5. Set the mill for between 1.5 and 3 minutes and turn on.
6. Take mill head out and place powder onto butchers' paper and then into a sample bag.
7. Repeat steps 2 – 6.